https://doi.org/10.5194/essd-2022-15
Preprint. Discussion started: 4 February 2022

Earth System Science Data Discussions
Open Access

A ten-year global monthly averaged terrestrial NEE inferred from the ACOS GOSAT v9 XCO_2 retrievals (GCAS2021)

Fei Jiang[1,2,4], Weimin Ju[1,2], Wei He[1], Mousong Wu[1], Hengmao Wang[1], Jun Wang[1], Mengwei Jia[1], Shuzhuang Feng[1], Lingyu Zhang[1], Jing M. Chen[1,3]

[1]Jiangsu Provincial Key Laboratory of Geographic Information Science and Technology, International Institute for Earth System Science, Nanjing University, Nanjing, 210023, China
[2]Jiangsu Center for Collaborative Innovation in Geographical Information Resource Development and Application, Nanjing, 210023, China
[3]Department of Geography, University of Toronto, Toronto, Ontario M5S3G3, Canada
[4]Frontiers Science Center for Critical Earth Material Cycling, Nanjing University, Nanjing, 210023, China

Correspondence to: Fei Jiang (jiangf@nju.edu.cn)

Abstract. A global gridded Net Ecosystem Exchange (NEE) of CO_2 dataset is vital in global and regional carbon cycle studies. Top-down atmospheric inversion is one of the major methods to estimate the global NEE, however, the existing global NEE datasets generated through inversion from conventional CO_2 observations have large uncertainties in places where observational data are sparse. Here, by assimilating the GOSAT ACOS v9 XCO_2 product, we generate a ten-year (2010–2019) global monthly terrestrial NEE dataset using the Global Carbon Assimilation System, version 2 (GCASv2), which is named as GCAS2021. It includes gridded (1°×1°), globally, latitudinally, and regionally aggregated prior and posterior NEE and ocean (OCN) fluxes, and prescribed wildfire (FIRE) and fossil fuel and cement (FFC) carbon emissions. Globally, the decadal mean NEE is -3.73±0.52 PgC yr^{-1}, with interannual amplitude of 2.73 PgC yr^{-1}. Combining the OCN flux, and FIRE and FFC emissions, the net biosphere flux (NBE) and atmospheric growth rate (AGR) as well as their inter-annual variabilities (IAVs) agree well with the estimates of Global Carbon Budget 2020. Regionally, our dateset shows that eastern North America, Amazon, Congo Basin, Europe, boreal forests, southern China and Southeast Asia are carbon sinks, while western US, African grasslands, Brazilian plateaus and parts of South Asia are carbon sources. In the TRANSCOM land regions, the NBEs of temperate N. America, northern Africa and boreal Asia are between the estimates of CMS-Flux NBE 2020 and CT2019B, and those in temperate Asia, Europe, and Southeast Asia are consistent with CMS-Flux NBE 2020 but significantly different from CT2019B. In the RECCAP2 regions, except for Africa and South Asia, the NBEs are comparable with the latest bottom-up estimate of Ciais et al. (2021). Compared with previous studies, the IAVs and seasonal cycles of NEE of this dataset could clearly reflect the impacts of extreme climates and large-scale climate anomalies on the carbon flux. The evaluations also show that the posterior CO_2 concentrations at remote sites and in regional scale, as well as on vertical CO_2 profiles in the Asia-Pacific region and the Amazon basin, are all consistent with independent CO_2 measurements from surface flask and aircraft CO_2 observations, indicating that this dataset captures surface carbon fluxes well. We believe that this dataset will contribute to regional or national-scale carbon cycle and carbon neutrality assessment, and carbon dynamics research. The dataset can be

https://doi.org/10.5194/essd-2022-15
Preprint. Discussion started: 4 February 2022

accessed at https://doi.org/10.5281/zenodo.5829774 (Jiang, 2022).

1 Introduction

Terrestrial ecosystem could uptake CO_2 from the atmosphere through photosynthesis and release CO_2 into the atmosphere through respiration. Its net carbon exchange (NEE) plays a very important role in regulating the atmospheric CO_2 concentration, thereby slowing down the global warming. However, NEE has significant spatial differences and inter-annual variations (IAV) (Bousquet et al., 2000; Piao et al., 2020). Therefore, accurately quantifying global and regional NEE and clarifying their drivers of IAV is a key scientific issue in global carbon cycle research, and a reliable global NEE dataset is vital for this research.

Until now, a series of global NEE or net biosphere exchange (NBE, = NEE + wildfire carbon emission) products like FLUXCOM (Jung et al., 2009), TRENDY (Sitch et al., 2015), Jena CarboScope (Rödenbeck et al., 2003), CT2019B (Jacobson et al., 2020), and CMS-Flux NBE 2020 (Liu et al., 2021), are available and widely used in different studies, which were created using data-driven machine learning methods, ecosystem models, or inversion models. Machine learning methods estimate global carbon flux by upscaling eddy covariance data (Zeng et al., 2020), ecosystem models simulate photosynthesis and respiration of ecosystems based on meteorological, soil, and land cover data and a series of parameters (Chen et al., 1999), and inversion models estimate surface CO_2 fluxes using the globally distributed atmospheric CO_2 observations and/or satellite retrievals of column averaged CO_2 dry air mole fraction (XCO_2) (Enting and Newsam, 1990; Gurney et al., 2002; Jiang et al., 2021). Different methods have their own advantages and disadvantages. The NEE estimated by top-down atmospheric inversions is determined by the density and accuracy of the CO_2 observations, the accuracy of modeled atmospheric transport, and knowledge of the prior uncertainties of the flux inventories (Liu et al., 2021). Generally, in situ and flask CO_2 observations have high precision, with measurement error lower than 0.2 ppm, however, the global distribution of flask or in-situ sites is extremely uneven, there are many sites over North America (N. America) and Europe, but very few sites over tropics, Africa, and southern oceans (Schuldt et al., 2020). Therefore, the inversions generally have robust performance on global or hemisphere scale (Houweling et al., 2015), but on regional scales, due to the uneven distribution of observations, the reliability of inversion results varies greatly in different regions (Peylin el al., 2013).

Satellite XCO_2 retrievals from the Greenhouse Gases Observing Satellite (GOSAT) (Kuze et al., 2009) and the Observing Carbon Observatory 2 (OCO-2) (Crisp et al., 2017) have much better spatial coverage (O'Dell et al., 2018) than ground-based observations. Although the accuracy of XCO_2 is relatively lower (~ 1 ppm, Kulawik et al., 2019) compared to flask and in-situ observations, and the response of XCO_2 to changes in the surface carbon flux is weaker, many inversion studies have proved that satellite XCO_2 retrievals could improve the estimates of surface carbon fluxes (e.g., Basu et al., 2013; Maksyutov et al., 2013; Saeki et al., 2013; Chevallier et al., 2014; Deng et al, 2016), especially for the fluxes in Africa, South America (S. America), and Asia, where the sparsity of the surface monitoring sites is most evident (Takagi et al., 2011). Wang et al. (2019)

https://doi.org/10.5194/essd-2022-15
Preprint. Discussion started: 4 February 2022

compared the NEE inferred from GOSAT and OCO-2 retrievals, and surface flask observations, and found that the performance of inversion with GOSAT data only was comparable with the one using surface observations. Moreover, studies also showed that with satellite XCO_2 retrievals, the inverted carbon flux could well reveal the impact of extreme droughts and large-scale climate anomalies on regional and continental terrestrial carbon dynamics (Liu et al., 2018; Deng et al, 2016; Detmers et al., 2015; Jiang et al., 2021).

By assimilating both GOSAT and OCO-2 XCO_2 retrievals, Liu et al. (2021) generated a global gridded monthly NBE product (i.e., CMS-Flux NBE 2020) using the NASA Carbon Monitoring System Flux (CMS-Flux) inversion framework (Liu et al., 2014, 2017, 2018; Bowman et al., 2017). This dataset spans over 2010–2018, in which the data from 2010-2014 and 2015-2018 were inferred from GOSAT XCO_2 and OCO-2 data, respectively. GOSAT and OCO-2 XCO_2 have large differences on spatial resolution and coverage, which may lead to discontinuities in the inversion results of certain regions. The ACOS GOSAT v9 XCO_2 data are now available on the NASA Goddard Earth Science Data and Information Services Center (GES-DISC), which spans from April 2009 to June 2020, and has been well bias corrected and quality filtered (Taylor et al., 2021).

In this study, based on the GOSAT v9 XCO_2 retrievals, we generate a 10-year global monthly NEE dataset from 2010 to 2019 (GCAS2021) using a well-constructed Global Carbon Assimilation System, version 2 (GCASv2) (Jiang et al., 2021; Wang et al., 2021a). Different from Liu et al. (2021), GCAS2021 focuses on NEE, because the wildfire (FIRE) emission was not optimized in this study. The optimized ocean flux and prescribed FIRE and fossil fuel and cement carbon (FFC) emissions are also included in this dataset. Users who want to use NBE data, could combine the NEE and FIRE emission by themselves. It is worth pointing out that since we have not optimized FIRE emissions, the optimized NEE may include compensation for the errors in FIRE emissions. This manuscript is organized as follows: Section 2 details the GOSAT retrievals, prior fluxes, and the GCASv2 system as well as uncertainty settings. Section 3 introduces the evaluation data and method, Section 4 briefly describes the dataset, Section 5 presents the characteristics of the dataset, including the estimates of global carbon budget and regional NEE as well as their IAVs, Section 6 details the evaluations results against independent CO_2 observations, and Section 7 gives a summary and the main conclusions.

2 Methods and data

2.1 The ACOS v9 GOSAT XCO_2 retrievals

The GOSAT satellite launched in 2009 (Kuze et al., 2009) was developed jointly by the National Institute for Environmental Studies (NIES), the Japanese Space Agency (JAXA) and the Ministry of the Environment (MOE) of Japan, which was designed to retrieve total column abundances of CO_2 and CH_4. In this study, the GOSAT XCO_2 retrieval is the ACOS Version 9.0 Level 2 Lite product (Taylor et al., 2021) at the pixel level during May 2009 - Dec 2019. The bias correction and quality filtering of this XCO_2 product have been evaluated using estimates derived from the Total Carbon Column Observing Network (TCCON)

https://doi.org/10.5194/essd-2022-15
Preprint. Discussion started: 4 February 2022

as well as values simulated from a suite of global atmospheric inverse modeling systems (models), the results show that the differences in XCO_2 between GOSAT v9 and both TCCON and models have an one sigma error of approximately 1 ppm for ocean-glint observations and 1 to 1.5 ppm for land observations, and globally, the mean biases are less than approximately 0.2 ppm (Taylor et al., 2021). Compared with its previous version (ACOS v7.3), the proportion of data with a 'good' XCO_2 quality flag has increased from 3.9 % in v7.3 to 5.4% in v9.

The GOSAT XCO_2 retrievals have a resolution of 10.5 km^2 at nadir. Considering the facts that the resolution of a global atmospheric transport model is significantly lower than that of XCO_2 retrievals, we re-grid the XCO_2 data into 1°×1° grid cells following the approach. The pixel level XCO_2 data are filtered with xco2_quality_flag. In each 1°×1° grid, only the XCO_2 with xco2_quality_flag equals 0 are selected and averaged. The xco2_quality_flag is a simple quality flag denoting science quality data (0=Good, 1=Bad), which is provided along with the XCO_2 product. The other variables in the XCO_2 product like column-averaging kernel, retrieval error, etc., which will be used in the calculations of simulated XCO_2, are also re-grided using this method.

2.2 Prior CO_2 fluxes

The prior carbon fluxes used in this study consist of terrestrial NEE, FIRE carbon emission, FFC carbon emission, and CO_2 exchanges over the ocean surface (OCN). NEE in 3-hour interval is simulated using the Boreal Ecosystems Productivity Simulator (BEPS) model, details about the BEPS simulations please refer to Chen et al. (2019). FIRE emission is directly obtained from the Global Fire Emissions Database, Version 4.1 (GFED4s) (van der Werf et al., 2017; Mu et al., 2011). FFC emission is an average of two products from Carbon Dioxide Information Analysis Center (CDIAC) (Andres et al., 2011) and Open-source Data Inventory of Anthropogenic CO_2 (ODIAC) (Oda et al., 2018), respectively. OCN flux is derived from the Takahashi et al. (2009) climatology of seawater pCO_2. Both FFC emission and OCN flux were downloaded from CT2019B (Jacobson et al., 2020). It should be noted that there are no data in the pCO_2-Clim product in many offshore areas like Japan Sea, Mediterranean, Gulf of Mexico, and East China Sea. Following Jiang et al. (2021), the fluxes in 2009 modeled using a global ocean circulation and biogeochemistry model is used to fill the no data areas. In addition, the CT2019B product is only until the beginning of 2019. OCN flux in 2019 is assumed to be the same as 2018. FFC emission is adjusted from the emission in 2018 by ratios of 2019/2018 in different countries or regions (Figure S1), which was calculated based on the 2018 and 2019 emissions compiled by the Global Carbon Budget 2020 (GCP2020, Friedlingstein et al., 2020).

2.3 The Global Carbon Assimilation System (GCAS, version 2)

The global monthly NEE dataset is inferred using the Global Carbon Assimilation System, version 2 (GCASv2), which was developed for estimating gridded surface carbon fluxes mainly using satellite XCO_2 retrievals (Jiang et al., 2021). In this system, the Model for Ozone and Related Chemical Tracers, version 4 (MOZART-4) (Emmons et al., 2010) was coupled to

https://doi.org/10.5194/essd-2022-15
Preprint. Discussion started: 4 February 2022

simulate 3-D atmospheric CO_2 concentrations, and the Ensemble square root filter (EnSRF) algorithm (Whitaker and Hamill, 2002) was used to implement the inversion of surface fluxes. GCASv2 runs cyclically, and in each cycle (DA window), we use a "two-step" calculation scheme to maintain quality conservation. First, the prior fluxes are optimized using XCO_2 data, and then, the optimized fluxes are put again into the MOZART-4 model to generate the initial condition (IC) of the next window. In order to reduce the representative error of XCO_2, a 'super-observation' approach is also adopted, in which a super-observation is generated by averaging all observations located within the same model grid within a DA window; and to reduce the impact of spurious correlations, a localization technique is employed to determine which super-observations will be used for the current grid's optimization, which is based on the correlation coefficient between the simulated concentration ensembles in each observation location and the perturbed fluxes in current model grids, and their distances. For details, please refer to Jiang et al. (2021).

In this study, GCASv2 was run from May 1, 2009 to Dec 31, 2019. The IC of 3-D CO_2 concentrations at 00:00 UTC May 1, 2009 was obtained from the product of CT2017. The first 8 months are considered as a spin-up run, and the results from Jan 1, 2010 to Dec 31, 2019 are analyzed and evaluated in this study. MOZART-4 is driven by the GEOS-5 meteorological fields, which has a spatial resolution of 1.9°×2.5°, and vertical level of 72 layers. MOZART-4 uses the same spatial resolution and the lowest 56 vertical levels of GEOS-5. Following Jiang et al. (2021), the model-data mismatch error of XCO_2 is constructed using the XCO_2 retrieval errors, which are provided along with the XCO_2 product and re-grided using the same method as described in section 2.1. All retrieval errors are also uniformly inflated by a factor of 1.9 in this study, but a lowest error is fixed as 1 ppm.

There are four state vectors combining schemes in GCASv2, including 1) only the BIO flux is treated as state vector and optimized, 2) both NEE and OCN flux are state vectors; 3) NEE, OCN flux and FCC emissions are optimized at the same time; and 4) only net flux is optimized. In this study, the second scheme was selected, both NEE and ocean flux are optimized, and the FIRE and FFC are prescribed. The perturbation of prior fluxes is described in Equation (1), where δ_i represents random perturbation samples, and is drawn from Gaussian distributions with mean zero and standard deviation of one. N is the ensemble size (here 50). λ is a set of scaling factors, which represents the uncertainty of each prior flux. X_{NEE}^b, X_{FIRE}^b, X_{FFC}^b, and X_{OCN}^b represent the prior fluxes of NEE, FIRE, FFC and OCN, respectively. In each model grid, λ_{NEE} and λ_{ocn} are set to be 6 and 10, respectively, which are corresponding to a global 1-δ uncertainty for NEE and OCN flux about 0.6 and 0.2 PgC yr^{-1}, respectively.

$$\boldsymbol{X_i^b} = \lambda_{NEE} \times \delta_{i,NEE} \times \boldsymbol{X_{NEE}^b} + \lambda_{ocn} \times \delta_{i,ocn} \times \boldsymbol{X_{OCN}^b} + \boldsymbol{X_{Fire}^b} + \boldsymbol{X_{FFC}^b}, i = 1, 2, \dots, N \quad (1)$$

https://doi.org/10.5194/essd-2022-15
Preprint. Discussion started: 4 February 2022

3 Evaluation data and method

Due to the huge difference of spatial scale between the inverted and directly observed fluxes, generally, it is impossible to directly validate the posterior NEE using observations, and instead, we indirectly evaluate the posterior flux by comparing the forward simulated atmospheric CO_2 mixing ratios against independent CO_2 measurements (e.g., Jiang et al., 2021; Wang et al., 2019; Feng et al., 2020). Therefore, a forward simulation using the MOZART-4 model and the posterior fluxes were conducted to create posterior CO_2 concentrations. The simulation period, model configuration of MOZART-4 as well as initial field are the same as the assimilation experiment as described in section 2.3.

Surface flask and aircraft CO_2 observations are used for these independent evaluations in this study, which were obtained from the obspack_co2_1_GLOBALVIEWplus_v6.0_2020-09-11 product (OBSPACKv6, Schuldt et al., 2020). OBSPACKv6 contains a collection of discrete (flask), programmable flask package (PFP) and quasi-continuous (in-situ) measurements at surface, tower, ship and aircraft sites contributed by national and universities laboratories around the world. In this study, surface flask CO_2 measurements (including surface pfp) from 74 sites, and aircraft measurements (including flask, PFP and in-situ measurement methods) from 50 sub-datasets, are selected to evaluate the posterior CO_2 concentrations. There are 148 surface flask and PFP sites of observations in OBSPACKv6. The 74 sites were selected according the following processes: 1) only the sites with data more than 7 years during 2010 – 2019 were selected (48 sites removed); 2) for one location, if there are observations from different institutes, only the data provided by the NOAA Global Monitoring Laboratory (with lab number of 1 in each filename) were selected (21 sites removed); 3) for one location, if both flask and PFP observations are available, only flask observations were adopted (1 site removed); 4) for PFP site, if there are observations at different heights, only the observations at the top level were used (1 site removed); and 5) during the evaluations, we find that MOZART-4 model is unable to capture the variations of CO_2 mixing ratios at BKT and LJO, thus these site were also removed. The locations of the 74 sites are shown in Figure 1 and the corresponding sites code as well as the information about latitude and longitude are listed in Table S2 in the Supporting Information.

There are 76 aircraft observation sites (independent data files) in OBSPACKv6. In this study, we chose observations from the Comprehensive Observation Network for Trace gases by Airliner (CONTRAIL) project (Machida et al., 2008, 2018; Matsueda et al., 2008, 2015), the HIAPER Pole-to-Pole Observations (HIPPO) programme (Wofsy et al., 2011), and the lower-troposphere greenhouse-gas sampling programme in the Amazon basin of the CARBAM project (Gatti et al., 2014, 2021) to further evaluate the posterior CO_2 concentrations. The CONTRAIL project measures CO_2 concentrations using Continuous CO_2 Measuring Equipment (CME) on two passenger aircrafts (Boeing 747-400 and 777-200ER), thus there are observations along flight paths (including level flight, taking off and landing) from Japan to N. America, to Europe, to Hawaii, to Australia, and to Southeast and South Asia (Figure 2). During the taking off and landing, vertical profiles of CO_2 concentrations near airports were observed. As shown in Figure 1, there are few surface observations over the Asia-Pacific region, especially in

https://doi.org/10.5194/essd-2022-15
Preprint. Discussion started: 4 February 2022

Southeast and South Asia, therefore, the CO_2 vertical profiles near 8 cities over the Asia-Pacific region are selected in this study. The 8 cities are Hong Kong, Singapore, Jakarta, Bangkok, Sydney, New Delhi, Shanghai, and Tokyo. The HIPPO programme completed aircraft measurements spanning the Pacific from 85 ° N to 67 ° S during the periods of March to April 2010, and June to September 2011, with vertical profiles every approximately 2.2 ° of latitude (Wofsy et al., 2011). The CARBAM project conducted vertical CO_2 measurements at 4 sites (i.e., ALF, RBA, SAN, TAB, and TEF) in the Amazon basin during 2010 ~ 2018 (Figure 2) with small aircrafts and PFP equipment. TAB was from 2010 to 2012, and TEF started in 2013. During the evaluation of this study, TAB and TEF are combined as one site of TAB_TEF. At each site, 1-3 spiral profiles from approximately 4420 m to about 300 m a.s.l. were observed in each month. It is worth noting that OBSPACKv6 only provides ALF, RBA, SAN and TAB observations from 2010 to 2012, the rest data were downloaded from Gatti et al. (2021). For the CONTRAIL vertical profiles, the observations between the heights of 2 and 6 km are used, because the data measured below 2000 m are highly affected by local emissions (Jiang et al., 2014) due to the frequently ascending and descending of aircrafts. And for the HIPPO and CARBAM observations, the data above 1 km are adopted.

Four basic statistical measures, i.e., mean bias (BIAS), mean absolute error (MAE), root mean square error (RMSE), and correlation coefficient (CORR), are calculated against the surface and aircraft CO_2 observations, respectively. The functions of these 4 basic statistical measures are expressed as:

$$BIAS = \frac{1}{M}\sum_{j=1}^{M}\left(x_j - y_j\right) = \bar{y} - \bar{x} \tag{2}$$

$$MAE = \frac{1}{M}\sum_{j=1}^{M}\left|x_j - y_j\right| \tag{3}$$

$$RMSE = \sqrt{\frac{1}{M}\sum_{j=1}^{M}\left(x_j - y_j\right)^2} \tag{4}$$

$$CORR = \frac{\sum_{j=1}^{M}(x_j-\bar{x})(y_j-\bar{y})}{\sqrt{\sum_{j=1}^{M}(x_j-\bar{x})^2}\sqrt{\sum_{j=1}^{M}(y_j-\bar{y})^2}} \tag{5}$$

where x_j and y_j denote the modeled and the observational values, respectively, at the jth out of M records, and the overbars denote averages. The BIAS, MAE, RMSE, and CORR reflect the overall model tendency, both the model bias and error variance, and the linear correspondence between the modeled and observational values, respectively.

4 Dataset description

GCAS2021 includes (1) monthly and annual prior and posterior NEE and OCN fluxes, and prescribed FIRE and FFC emissions in a global spatial resolution of 1°×1°; (2) globally, latitudinally, and regionally aggregated monthly and annual posterior NEE and NBE, and their uncertainties; and (3) weekly gridded ensemble members of posterior NEE and OCN fluxes. The regional fluxes are aggregated both in the TRANSCOM (Gurney et al., 2003) and the REgional Carbon Cycle Assessment and Processes

https://doi.org/10.5194/essd-2022-15
Preprint. Discussion started: 4 February 2022

Open Access Earth System Science Data Discussions

Project (RECCAP2, Ciais et al., 2020) regions (Figure 3). The latitudinal fluxes are aggregated in northern mid-high latitudes (> 30° N, NL), low latitudes (30° S ~ 30° N, TL), and southern middle latitudes (<30° N, SL). The weekly gridded ensemble members could be used for calculating the posterior uncertainties based on user defined regional masks. We also provide a Fortran program for the calculation of posterior uncertainties. The gridded data are in NETCDF-3 format, while the regional aggregated data are in xlsx format.

5 Characteristics of the dataset

5.1 Global carbon budgets

Table 1 presents the year-by-year and decadal averaged posterior global carbon budgets during 2010 ~ 2019 of this study. The global annual NEE is in the range of -2.51±0.53 to -5.24±0.50 PgC yr^{-1} (negative means absorbing CO_2 from the atmosphere, and positive means releasing CO_2 to the atmosphere). The year of 2011 has the largest land sink in the decade, while the year of 2016 has the weakest one, with interannual amplitude reaching 2.73 PgC yr^{-1}. On average, the decadal mean NEE is -3.73±0.52 PgC yr^{-1}. The OCN flux has an overall increase trend from 2010 to 2009, with a mean of -2.64±0.16 PgC yr^{-1}. Figure 4 presents a comparison between the estimates of this study and GCP2020 (Friedlingstein et al., 2020). There are large differences for the land-use and land-cover change (LULLC) carbon emissions between this study and GCP2020, we directly use the FIRE emission from GFED 4.1s as prescribed land-use emission, while GCP2020 uses an average of three bookkeeping models (Houghton et al., 2017; Hansis et al., 2015; Gasser et al., 2020), which account for changes in all carbon pools affected by LULCC. Therefore, we compared the NBE (excluding FFC emissions) and atmospheric growth rate (AGR) between this study and GCP2020. The interannual changes of global NBE and AGR of this study match well with the estimates of GCP2020, with CORR of 0.75 and 0.88, BIAS (GCAS2021 minus GCP2020) of 0.15 and 0.25 PgC yr^{-1}, and MAE of 0.51 and 0.40 PgC yr^{-1}, respectively. For the prior fluxes, the CORR, BIAS, and MAE of NBE and AGR compared against the GCP2020 estimates are 0.16 and 0.49, -0.51 and 0.09 PgC yr^{-1}, and 0.63 and 1.10 PgC yr^{-1} (Figure S2). These indicate that the estimate of global carbon budgets has been significantly improved after constrained by the GOSAT retrievals.

5.2 Annual NEE averaged from 2010-2019

Figure 5 shows the distributions of the mean posterior annual NEE during 2010 - 2019. Carbon uptakes mainly occur over eastern N. America, Amazon, Congo Basin, Europe, boreal forests, southern China, and southeast Asia; and carbon releases mainly occur in western N. America (main western US), the East African and Ethiopian Plateaus and the Sahel region (mainly the grasslands in Africa), the Brazilian plateau, and parts of South Asia. Compared with the prior NEE, the land sinks in western N. America, most S. America, the grasslands in Africa, most East and South Asia, and eastern Siberia are decreased, while the sinks in eastern N. America, Europe, and western Siberia are significantly increased (Figure S3). In N. America, the distribution

https://doi.org/10.5194/essd-2022-15
Preprint. Discussion started: 4 February 2022

of NEE constraint with GOSAT XCO_2 agrees well with a recent regional inversion using surface CO_2 and $^{14}CO_2$ measurements, which also shown significant sources over western US and sinks over central and eastern US (Basu et al., 2020). By using the Community Land Model (CLM5.0) and a Data Assimilation Research Testbed (DART) that assimilated with remotely sensed observations of leaf area and above-ground biomass, Raczka et al. (2021) simulated the NEE over western US and also found that there are large areas with carbon release. The western US is dominated by natural lands, which is particularly vulnerable to forest mortality from droughts, insect attacks, and wildfires, Ghimire et al. (2015) found large carbon release legacy from bark beetle outbreaks across western US. In addition, the ageing and decline of forest may be another reason for the carbon release in western US (Sleeter et al., 2018). The significant sources of NEE in the grasslands of Africa are consistent with previous top-down estimates based on satellite retrievals (Palmer et al., 2019) and surface CO_2 measurements (Valentini et al., 2014). Many observations based on the eddy covariance also reported carbon sources of NEE in the savanna grassland of West and South Africa (e.g., Veenendaal et al., 2004; Räsänen et al., 2017; Quansah et al., 2015). The significant increase of carbon release in the grasslands of Africa may be related to the underestimates of carbon emissions from small fires in GFED 4s. The FIRE emission in GFED 4s was estimated based on global burned area, which were from coarse spatial-resolution sensors. Ramo et al. (2021) shown that coarse sensers are unsuitable for detecting small fires that burn only a fraction of a satellite pixel, and pointed out that the FIRE emission of Africa in GFED 4s was underestimated by about 31% in 2016.

Table 2 lists the aggregated mean posterior annual NEE, NBE and FIRE emissions during the 1- years for the 11 TRANSCOM regions and the 10 RECCAP2 regions. Compared with the prior NEE, the absolute relative changes in most TRANSCOM regions are greater than 50% (Figure S4) after constrained with GOSAT data. In all regions, the aggregated posterior NEE are negative, indicating a carbon sink in each region. For the 11 TRANSCOM regions, we estimate that Europe has the strongest NEE, followed by boreal Asia, tropical S. America, and northern Africa has the weakest NEE. Among the 10 RECCAP2 regions, Russia's NEE is the strongest, followed by N. America and Europe, and West Asia's NEE is the weakest. It is worth noting that the Europe's NEE in the TRANSCOM region is twice that in RECCAP2. This is because the coverage of Europe is different in TRANSCOM and RECCAP2, the former includes the entire European continent, while the latter does not include European Russia.

Figure 6 shows a comparison between the results of this study and previous studies for both the TRANSCOM and RECCAP2 regions. For the TRANSCOM region, we compared our estimates with the products from the CMS-Flux (CMS-Flux NBE 2020, Liu et al., 2021) and CarbonTracker (CT2019B, Jacobson et al., 2020) systems. CMS-Flux NBE 2020 is a product for the period of 2010-2018, in which the results of 2010-2014 was inverted from the GOSAT XCO_2 v7.3, and the rests were inverted from the OCO-2 XCO_2 v9 retrievals. CT2019B is a product inverted from global surface, tower and aircraft CO_2 measurements. CMS-Flux NBE 2020 only presented the NBE results, and the FFC emission used in this study and CT2019 are also different. Therefore, we compared the estimates of NBE in each region. As shown in Figure 6a, in temperate N.

https://doi.org/10.5194/essd-2022-15
Preprint. Discussion started: 4 February 2022

America, northern Africa, boreal Asia, the estimates of this study are between the results of CMS-Flux NBE 2020 and CT2019B; in temperate Asia, Europe, and tropical Asia, our estimates are very close to CMS-Flux, but are significant differences with CT2019B, conversely, in Australia, our estimates are very consistent with CT2019B, but are significantly different from CMS-Flux. In tropical S. America, our result shows a strong carbon sink, which is consistent with previous mean annual biomass sink estimate of -0.39 ± 0.10 PgC yr^{-1} in Amazon during the 1980–2004 period based on repeated censuses at a widespread forest plot network (Phillips et al., 2009) and is roughly consistent with a regional inversion in a wet year of -0.25 PgC yr^{-1} based on aircraft CO_2 measurements (Gatti et al., 2014), while CMS-Flux NBE 2020 and CT2019B are both carbon sources. On the contrary, in temperate S. America, our result shows a weak carbon source, while the other two are both carbon sinks. In addition, in southern Africa, our estimate is also significantly different from them, we show strong carbon source, while CMS-Flux NBE 2020 and CT2019B show weak sink and source, respectively.

Based on inventory data of carbon-stock changes and satellite estimates of biomass changes where inventory data are missing, Ciais et al. (2021) gave a state-of-the-art estimate for the NBE of the RECCAP2 regions for the period of 2000-2009, which was calculated by taking the sum of the carbon-stock change and lateral carbon fluxes from crop and wood trade, and riverine-carbon export to the ocean. Figure 6b shows a comparison between this study and Ciais et al. (2021). Although the inverted NBE is not completely equivalent to the land sink obtained by the bottom-up method, generally, to reconcile top-down and bottom-up results, the inverted NBE should be adjusted with the lateral transport of reduced carbon compounds (RCC) and carbon release from net imported products (Ciais et al., 2008; Jiang et al., 2016). Overall, except for Africa and South Asia, the NBE estimated in this study and Ciais et al. (2021) are comparable. In Africa, we show a strong carbon source of 0.87±0.27 PgC yr^{-1}, while Ciais et al. (2021) reported a very weak sink of –0.07 ± 0.29 PgC yr^{-1}. Until now, there are still big differences in top-down estimates of African NBE in different studies. Generally, the estimates based on surface CO_2 measurements show carbon sinks or weak source, which are mainly in the range of -0.26 to 0.32 PgC yr^{-1}, Valentitni et al., 2014; Jacobson et al., 2020), while the estimates from satellite XCO_2 retrievals report strong carbon sources, with values mainly in the range of 0.61 to 2.2 PgC yr^{-1} (Liu et al., 2021; Palmer et al., 2019). Although the estimates based on surface measurements are much closer to Ciais et al. (2021)'s result, the surface CO_2 observation sites in Africa are very sparse, there are only 4 stations over the African continent and 2 stations located in adjacent islands, indicating that the constraints from surface measurements are very poor, and the inverted fluxes often reflect the prior fluxes used in these inversions (Valentitni et al., 2014). In our prior flux, the NBE in Africa is 0.34 PgC yr^{-1}, that is consistent with above surface-based estimates. This indicates that the strong carbon source is almost constrained from satellite XCO_2. Since there is no TCCON site in Africa, which is usually used to verify and correct the satellite XCO_2 retrievals, leading larger uncertainties in the XCO_2 products, thus probably resulting in an overestimation of the surface flux. In South Asia, we show a very weak sink of -0.05±0.10 PgC yr^{-1}, while Ciais et al. (2021) presented a moderate sink of -0.25 PgC yr^{-1}. Based on bottom-up and top-down methods, there

https://doi.org/10.5194/essd-2022-15
Preprint. Discussion started: 4 February 2022

have been many studies on NBE in South Asia in the past. Overall, the bottom-up estimates are in the range of -0.01 ~ -0.25 PgC yr^{-1} (Cervarich et al., 2016; Ciais et al., 2021; Nayak et al., 2015; Gahlot et al., 2017; Patra et al., 2013), while the top-down estimates are in the range of 0.04 ~ -0.37 PgC yr^{-1} (Patra et al., 2013; Thompson et al., 2016; Cervarich et al., 2016; Niwa et al. 2012; Jiang et al., 2014; Swathi et al. 2021). Our result for South Asia is in the range of these previous studies.

5.3 Interannual variations and seasonal cycles

Figure 7a, b, and c show interannual variations (IAV) of the NEE in the NL, TL and SL, respectively. In NL, the IAV of NEE is relatively small, with an interannual amplitude of 1.09 ± 0.50 PgC/yr. The smallest year of NEE appeared in 2018, which was -1.87 ± 0.38 PgC/yr, and the largest year appeared in 2014, with value of -2.91 ± 0.33 PgC yr^{-1}. In TL, the inter-annual variability is very large, with the biggest NEE in 2011 of -2.27 ± 0.33 PgC yr^{-1} and the smallest NEE in 2016 only -0.31 ± 0.41 PgC yr^{-1}. The interannual amplitude of NEE in TL is nearly twice that of NL, which reaches 1.96 ± 0.53 PgC yr^{-1}. The strongest carbon sink in 2011 and weakest sink in 2016 are related to the strongest 2011 La Niña and 2015/2016 El Niño events, respectively, which is in good agreement with many previous findings (Liu et al. 2017; Bastos et al. 2018; Wang et al., 2018; Koren et al., 2018). Bastos et al. (2018) showed a smaller difference of carbon fluxes between 2015 and 2011 using both bottom-up and top-down approaches, which was in the range of 0.7 ~ 1.9 PgC yr^{-1}. With the constraints of GOSAT and OCO-2 XCO_2, Liu et al. (2017) found that relative to the 2011 La Niña, the pantropical biosphere released 2.5 ± 0.34 PgC more carbon into the atmosphere in 2015, and during the peak 2015–2016 El Niño between May 2015 and April 2016, the more released carbon reached 3.3 ± 0.34 PgC. In this dataset, the changes of carbon flux between 2011 La Niña and 2015-2016 El Niño events in the pantropical area are lower than the estimates of Liu et al. (2017), but close to Bastos et al. (2018). We estimate the change of NBE between 2015 and 2011 is 1.59 ± 0.34 PgC yr^{-1}, and the peak period of 2015-2016 El Niño released 2.79 PgC more than in 2011 (Figure S5). In addition, it also could be found there are weak carbon sinks in 2010 and 2019 in TL. There have been many studies on the decline of carbon sinks in tropical regions in 2010 (van der Laan-Luijkx et al., 2015; Doughty et al., 2015; Gatti et al., 2014). In 2019, the decrease of NEE may be related to the Indian Ocean Dipole event, which has significantly reduced the carbon uptakes over southern China, Indo-China peninsula, and Australia (Wang et al., 2021b). In SL, due to the small land area, its NEE is an order of magnitude lower than the other two regions. It could be found that there is a continuous decreasing trend. On average, the NEE in NL, TL, and SL during this decade are -2.33 ± 0.35, -1.25 ± 0.38, and -0.05 ± 0.07 PgC yr^{-1}, which account for 62.6%, 33.4% and 1.4% of the global total land NEE, respectively, indicating that the global land NEE is dominated by the NEE in NL. However, the correlation coefficients for the IAVs of NEE between these three regions and the global land are 0.57, 0.86, and 0.37, respectively, indicating that the IAV of global NEE is dominated by its inter-annual changes in TL.

In Figure 8, we further present the IAVs and seasonal cycles of NEE in the 11 TRANSCOM regions. Since there are some overlaps between the TRANSCOM and RECCAP2 regions, for example, the N. America region in RECCAP2 is almost the

https://doi.org/10.5194/essd-2022-15
Preprint. Discussion started: 4 February 2022

sum of the boreal and temperate N. America, the Africa region in RECCAP2 is the sum of the northern and southern Africa in TRANSCOM. Besides, the IAVs of NEE in some regions of RECCAP2 like Russia, East Asia are dominated by the NEE changes in corresponding regions in TRANSCOM. Therefore, here we only analyze the annual and monthly changes of NEE in the TRANSCOM regions. The differences for the IAVs between the prior and posterior NEE in each region are shown in Figure S6.

There are significant differences in the IAVs of annual NEE in each region. For example, in boreal N. America, there is the weakest sink in 2016 and the strongest sink in 2017, while in temperate N. America, the weakest sink occurs in 2018, and the strongest in 2010; Europe has the weakest sink in 2018, but the strongest sink is in 2014. For the interannual amplitudes, temperate N. America, tropical S. America, southern Africa, Australia and Europe have relatively larger interannual amplitudes, with values above 0.6 PgC yr^{-1}; in temperate S. America, boreal Asia, northern Africa, temperate Asia and tropical Asia, the interannual amplitudes are comparable, ranging from 0.33 to 0.40 PgC yr^{-1}, while in boreal N. America, it has the smallest interannual amplitude of 0.22 PgC yr^{-1}. Except for boreal N. America, boreal Asia, and Europe, the interannual amplitudes in other regions are larger than their ten-year averaged carbon sinks, especially in the temperate S. America, northern and southern Africa, and Australia, their inter-annual amplitudes of NEE reach more than 5 times of the mean carbon sinks.

For the seasonal cycles, the northern middle and high latitudinal regions have similar pattern, with carbon sources during the cold season (from October to April), and carbon sinks during the warm season (from May to September). In the cold season, the difference of carbon releases in different regions is relatively small, but in the warm season, the intensity of carbon sinks in different regions is significantly different, and the months in which the strongest carbon sinks appear are also different. Boreal Asia, temperate and boreal N. America have the strongest sinks in July, Europe has the strongest one in June, while temperate Asia has the strongest in August. For the southern lands, southern Africa and temperate S. America have a similar seasonal cycle. their carbon sources occur from July to about December, with peak in October, and carbon sinks appear from January to May. In Australia, the carbon sinks mainly occur from March to October. In tropics, northern Africa has an opposite seasonal cycle with its adjacent region of southern Africa, its carbon sink occurs during June to November. The seasonal cycles in tropical Asia and tropical S. America are also nearly opposite. Tropical S. America has the strongest sink in September and October, while tropical Asia has the strongest carbon release in October. In general, the tropical regions have a smaller seasonal amplitude, while the high latitudes have a larger seasonal amplitude. In boreal Asia and Europe, their seasonal amplitudes reach 1.17 and 0.96 PgC mo^{-1}, respectively, while in tropical Asia and tropical S. America, the seasonal amplitudes are only about 0.12 PgC mo^{-1}. The same region has basically similar seasonal cycles in different years, but the intensity of its carbon sources and sinks, the time of transition from carbon source to carbon sink, and the months with the strongest sink or source are also significantly different in different years. For example, in tropical Asia, the carbon sources from January to April in 2010 and 2016 are significantly stronger than those in normal years; in temperate N. America, the carbon sinks in the spring

https://doi.org/10.5194/essd-2022-15
Preprint. Discussion started: 4 February 2022

of 2012 are significantly stronger than normal, but the carbon sinks in the summer are significantly weaker than normal.

Generally, the IAVs of annual NEE and seasonal cycles are related to large-scale climate anomalies and regional extreme climate events like droughts, heatwaves and precipitation, which have been widely studied around the world (e.g., Ciais et al., 2005; Betts et al., 2020; Bastos et al., 2018; Koren et al., 2018; Reichstein et al., 2013; Frank et al., 2015; Zhao and Running, 2010). Evidences have shown that severe drought events occurred in Amazon in 2010 (Potter et al., 2011; Doughty et al., 2015), Europe in 2010 (Bastos et al., 2020a), 2012 (He et al., 2019) and 2018 (Bastos et al., 2020b; Graf et al., 2020; Wang et al., 2020), the Unite States in 2011-2012 (He et al., 2018; Wolf et al., 2016) and 2018 (Li et al., 2020), and Australia in 2019 (Byrne et al., 2021) had caused significant reductions of terrestrial carbon uptakes. Accordingly, as shown in Figure 8, the NEE in this dataset are also much smaller in those years and regions compared with the normal year. Specially, in 2012, the contiguous United States experienced exceptionally warm temperatures and the most severe drought since the Dust Bowl era of the 1930s, Wolf et al. (2016) found that the warm spring reduced the impact of the summer drought on net annual carbon uptake across the United States. As mentioned above, our dataset also shows the significant increase of carbon sink in the spring of 2012, and large decrease during the summertime in temperate N. America. In the summer 2010, western Russia was hit by an extraordinary heat wave, with the region experiencing by far the warmest July since records began (Otto, et al., 2012), correspondingly, we find that in our dataset, the carbon sink in boreal Asia in July 2010 is the weakest in this decade, and the areas with significant positive anomaly of NEE (source increase) are mainly in western Russia (Figure S7). The strong El Niño events in 2015 and 2016 led to a significant reduction in carbon sinks in the pantropical regions, and many regions even turned to carbon sources (Liu et al., 2017; Bastos et al., 2018). Clearly, during 2015 – 2016, the inverted carbon sink in this study is much weaker than normal years in tropical S. America and tropical Asia, and it turns to carbon sources in northern and southern Africa. These indicate that this NEE dataset could clearly reveal the impact of climate extremes on carbon uptakes, thus it will benefit for the studies of the trends and drivers of carbon flux in different regions of the world.

6 Evaluations

6.1 Against surface flask observations

As shown in section 3, surface flask observations from 74 sites are used to evaluate the inversion results. the modeled CO_2 concentrations were extracted from the simulated 3-hour interval 3-D CO_2 fields according to the locations, time and heights of each observation. It should be noted that the records with absolute errors greater than 10 ppm were removed, which are considered to be lack of regional representativeness. Due to the low spatial resolution (1.9°×2.5°) of our model, we cannot reproduce such observations. Figure 9 shows the comparisons between the posterior CO_2 concentrations and surface flask CO_2 measurements. At most sites located in ocean areas, tropical lands, and southern lands, the BIAS is within ±0.5 ppm, and MAE lower than 1 ppm. In the northern mid-high latitudes, BIAS of some stations is higher than ±1.0 ppm, and MAE of almost all

https://doi.org/10.5194/essd-2022-15
Preprint. Discussion started: 4 February 2022

stations is higher than 1.5 ppm (Table S1). The global mean BIAS, MAE, and RMSE are 0.36, 1.76, and 2.28 ppm. The CORR of each site are in the range of 0.86 and 1, with global mean of 0.96.

The higher deviations in the northern mid-high latitudes, especially in temperate N. America and Europe, are probably due to the mismatch of spatial and temporal representativeness between the observations and simulations. In order to further increase the spatial and temporal representativeness of the observations, regional and monthly mean observed and modeled concentrations in 7 land regions are compared. As shown in Figure 1, the 7 regions are high latitudes (> 60° N), N. America, S. America, Europe, East Asia, Africa, and Australia. There are 8 sites in the high latitudes, 19 sites in N. America, 9 sites in Europe, 5 sites in East Asia, 3 sites in S. America, 5 sites in Africa, and 4 sites in Australia (Figure 1, Table S1). Figure 10 shows the time series of the monthly observed and modelled CO_2 concentrations in the 7 regions. Besides, the Mauna Loa Observatory (MLO) in Hawaii is a global background site, the comparisons of monthly mean concentrations at MLO are also shown in Figure 10. Clearly, the modeled regional and monthly mean CO_2 concentrations agree well with the observations. The mean BIAS are in the range of 0.1 to 0.56 ppm, and MAE and RMSE are in the range of 0.42 ~ 1.46, and 0.52 ~ 1.73 ppm, respectively. In S. America, Africa, and Australia, the posterior CO_2 concentrations are very consistent with the observations, with BIAS only in the range of 0.1 ~ 0.24 ppm, and MAE about 0.5 ppm. Among these regions, the deviations in Europe and high latitude regions are relatively larger, with MAE greater 1.4 ppm and RMSE about 1.7 ppm. Significant positive biases mainly occur during the winter. This is understandable, because in the winter at high latitudes, satellite observations are very scarce, leading to very insufficient constraints on the winter carbon flux. This indicates that there may be an overestimation of carbon releases at high latitudes in winter. At MLO, the simulations also agree well with the observations, with BIAS, MAE, and RMSE of 0.2, 0.46, and 0.57 ppm, respectively.

6.2 Against aircraft measurements

We further evaluate the posterior CO_2 concentrations against the aircraft observations. First, the posterior CO_2 were extracted from the simulated CO_2 fields according to the locations, time and heights of each aircraft observation, and then, both the observed and modeled CO_2 concentrations were divided into 14 layers: 1000–1500, 1500–2000, 2000–2500, 2500–3000, 3000–3500, 3500–4000, 4000–4500, 4500–5000, 5000–5500, 5500–6000, 6000–7000, 7000–8000, 8000–9000 and above 9000 m (CONTRAIL only 3-10 layer, and GATTI2014 only 1-8 layer). Monthly mean observed and modeled CO_2 concentrations at each height were calculated and compared for the CONTRAIL and GATTI2014 profiles. For comparisons against the HIPPO observations, the data were further divided into 2° interval along longitudinal direction, and all data in each layer and 2° of latitudes were averaged.

Figure 11 and 12 shows the evaluation results of monthly mean profiles in the 8 cities over the Asia-Pacific region, and at the 4 sites in the Amazon basin, respectively. Overall, the deviations between the simulations and observations decrease with height. In the Asia-Pacific region, the BIAS are basically within ±0.5 ppm, and most MAE are smaller than 1 ppm,

https://doi.org/10.5194/essd-2022-15
Preprint. Discussion started: 4 February 2022

especially in Southeast Asia, indicating that we have a good estimate of NEE in this area. Shanghai and New Delhi have relatively larger MAE and RMSE, with MAE about 1.5 ppm, and RMSE existing 2 ppm in the lowest level, probably due to the fact that Shanghai and New Delhi are one of the largest cities in China and India, respectively, and have very strong anthropogenic CO_2 emissions, which may affect the performance of the MOZART model. In the Amazon basin, the simulated CO_2 profiles also agree well with the observations, with BIAS and MAE basically lower than 1 and 1.5 ppm, respectively. Except for the lowest level at ALF, all BIAS are positive, with a total average of 0.2 ppm at 1000 ~ 1500 m heights, indicating that the strong carbon sink in tropical S. America estimated in this study are reasonable.

Figure 13 shows the comparisons against the HIPPO observations at different heights and latitudes. Overall, most BIAS are within ±0.5 ppm, showing a good agreement between the simulations and observations. Relatively large BIAS occurs over northern high latitudes, which is consistent with the comparisons against the surface observations as shown in Figure 10, and also reveals an overestimation of carbon releases at high latitudes.

7 Summary

A global NEE dataset is essential for estimating the regional terrestrial carbon budget and understanding the responses of carbon fluxes on extreme climates. Here, by assimilating the GOSAT ACOS v9 XCO_2 product, we generate a ten-year global monthly terrestrial NEE dataset from 2010 to 2019 (GCAS2021) using the GCASv2 system. GCAS2021 includes monthly and annual gridded (1°×1°) prior and posterior NEE and OCN flux, and prescribed FIRE and FFC emissions, and globally, latitudinally, and regionally aggregated fluxes and their uncertainties. Globally, the decadal mean NBE and AGR as well as their IAVs match well with the estimates of GCP2020. Regionally, our product shows carbon sinks over eastern N. America, Amazon, Congo Basin, Europe, boreal forests, southern China, and southeast Asia, and carbon sources over western US, African grasslands, Brazilian plateau, and parts of South Asia. In the 11 TRANSCOM land regions, the NBEs of temperate N. America, northern Africa and boreal Asia are between the results of CMS-Flux NBE 2020 and CT2019B, and those in temperate Asia, Europe, and tropical Asia are very close to CMS-Flux NBE 2020 but significantly different from CT2019B. In the RECCAP2 regions, except for Africa and South Asia, the NBEs are comparable with the latest bottom-up estimate of Ciais et al. (2021). The IAVs and seasonal cycles of NEE could clearly reflect the impact of extreme climates or large-scale climate anomalies. We also qualitatively evaluate the NEE estimates by comparing posterior CO_2 concentrations with independent CO_2 measurements from surface flask and aircraft CO_2 observations, and the results show that the simulated remote site and regional average CO_2 concentrations, as well as the vertical CO_2 profiles, are all consistent with the observations. We believe that this dataset will be useful in the estimates of regional or national-scale terrestrial carbon budgets, the study of carbon sink evolution mechanisms, the evaluation of ecosystem models, and the assessments of carbon neutrality strategies.

Data availability

The GCAS2021 data are available at https://doi.org/10.5281/zenodo.5829774 (Jiang, 2022). The regional aggregated fluxes are provided as xlsx files with file size ~135 KB, the gridded fluxes and ensemble members are provided in NetCDF format with file size ~82 MB and 5.8 GB, respectively.

Author contributions

FJ, JC and WJ designed the research; FJ run the model, analyzed the results and wrote the paper; HW handled the GOSAT XCO_2 retrievals; WH analyzed the products of CMS-Flux and CT2019B; WJ run the BEPS model; MJ, SF, and LZ participated in evaluations; JC, WJ, MW and HW participated in the discussions of the inversion results and provided inputs on the paper for revision before submission.

Competing interests

The authors declare that they have no conflict of interest.

Acknowledgements

This work is supported by the National Key R&D Program of China (Grant No: 2020YFA0607504 and 2016YFA0600204), and the Fundamental Research Funds for the Central Universities (Grant No: 090414380030, 090414380027, and 0207-14380179). We acknowledge all atmospheric data providers to obspack_co2_1_GLOBALVIEWplus_v6.0_2020-09-11. CarbonTracker CT2019B results are provided by NOAA ESRL, Boulder, Colorado, USA, from the website at http://carbontracker.noaa.gov. The GOSAT data are produced by the OCO project at the Jet Propulsion Laboratory, California Institute of Technology, and obtained from the data archive at the NASA Goddard Earth Science Data and Information Services Center. We are also grateful to the High-Performance Computing Center (HPCC) of Nanjing University for doing the numerical calculations in this paper on its blade cluster system.

References

Andres, R. J., Gregg, J. S., Losey, L., Marland, G. and Boden, T. A.: Monthly, global emissions of carbon dioxide from fossil fuel consumption. Tellus B, 63(3), 309–327, https://doi.org/10.1111/j.1600-0889.2011.00530.x, 2011.

Bastos, A., Friedlingstein, P., Sitch, S., Chen, C., Mialon, A., Wigneron, J.-P., Arora, V. K., Briggs, P. R., Canadell, J. G., and Ciais, P.: Impact of the 2015/2016 El Niño on the terrestrial carbon cycle constrained by bottom-up and top-down approaches. Philos. T. Rosy Soc. B, 373(1760), 20170304, https://doi.org/10.1098/rstb.2017.0304, 2018.

Bastos, A., Fu, Z., Ciais, P., Friedlingstein, P., Sitch, S., Pongratz, J., Weber, U., Reichstein, M., Anthoni, P., Arneth, A., Haverd, V., Jain, A., Joetzjer, E., Knauer, J., Lienert, S., Loughran, T., McGuire, P. C., Obermeier, W., Padrón, R. S., Shi, H., Tian, H., Viovy, N., and Zaehle, S.: Impacts of extreme summers on European ecosystems: a comparative analysis of 2003, 2010 and 2018, Philos. T. Rosy Soc. B, 375, 20190507, https://doi.org/10.1098/rstb.2019.0507, 2020a.

Bastos, A., Ciais, P., Friedlingstein, P., Sitch, S., Pongratz, J., Fan, L., Wigneron, J., Weber, U., Reichstein, M., Fu, Z., Anthoni, P., Arneth, A., Haverd, V., Jain, A. K., Joetzjer, E., Knauer, J., Lienert, S., Loughran, T., McGuire, P. C., Tian, H., Viovy, N., and Zaehle, S.: Direct and seasonal legacy effects of the 2018 heat wave and drought on European ecosystem productivity, Sci. Adv., 6, eaba2724, https://doi.org/10.1126/sciadv.aba2724, 2020b.

Basu S., Lehman S. J., Miller J. B., Andrews A. E., Sweeney C., Gurney K. R., Xu X., Southon J., and Tans P. P.: Estimating US fossil fuel CO_2 emissions from measurements of ^{14}C in atmospheric CO_2, Proc. Natl. Acad. Sci. U. S. A., 117 (24), 13300–13307, https://doi.org/10.1073/pnas.1919032117, 2020.

Basu, S., Guerlet, S., Butz, A., Houweling, S., Hasekamp, O., Aben, I., Krummel, P., Steele, P., Langenfelds, R., Torn, M., Biraud, S., Stephens, B., Andrews, A., and Worthy, D.: Global CO_2 fluxes estimated from GOSAT retrievals of total column CO_2, Atmos. Chem. Phys., 13, 8695–8717, https://doi.org/10.5194/acp-13-8695-2013, 2013.

Betts, R.A., Burton, C.A., Feely, R.A., Collins, M., Jones, C.D. and Wiltshire, A.J.: ENSO and the Carbon Cycle. In El Niño Southern Oscillation in a Changing Climate (eds M.J. McPhaden, A. Santoso and W. Cai). https://doi.org/10.1002/9781119548164.ch20, 2020.

Bousquet, P., Peylin, P., Ciais, P., Le Quéré, C., Friedlingstein, P., and Tans, P. P.: Regional Changes in Carbon Dioxide Fluxes of Land and Oceans Since 1980, Science, 290, 1342–1346, https://doi.org/10.1126/science.290.5495.1342, 2000.

Bowman, K. W., Liu, J., Bloom, A. A., Parazoo, N. C., Lee, M., Jiang, Z., Menemenlis, D., Gierach, M. M., Collatz, G. J., Gurney, K. R., and Wunch, D.: Global and Brazilian carbon response to El Niño Modoki 2011–2010, Earth Space Sci., 4, 637–660, https://doi.org/10.1002/2016EA000204, 2017.

Byrne, B., Liu, J., Lee, M., Yin, Y., Bowman, K. W., Miyazaki, K., Norton, A. J., Joiner, J., Pollard, D. F., Griffith, D. W. T., Velazco, V. A., Deutscher, N. M., Jones, N. B., and Paton-Walsh, C.: The carbon cycle of southeast Australia during 2019-2020: Drought, fires and subsequent recovery, EarthArxiv, https://doi.org/10.31223/X5PP6S, 2021.

Cervarich, M., Shu, S., Jain, A. K., Arneth, A., Canadell, J., Friedlingstein, P., Houghton, R. A., Kato, E., Koven, C., Patra, P., Poulter, B., Sitch, S., Stocker, B., Viovy, N., Wiltshire, A., and Zeng, N.: The terrestrial carbon budget of South and Southeast Asia. Environ. Res. Lett., 11. https://doi.org/10.1088/1748-9326/11/10/105006, 2016.

Chen, J. M., Ju, W., Ciais, P., Viovy, N., Liu, R. G., Liu, Y., and Lu, X. H.: Vegetation structural change since 1981 significantly enhanced the terrestrial carbon sink. Nat. Commun., 10, 4259, https://doi.org/10.1038/s41467-019-12257-8, 2019.

Chen, J. M., Liu, J., Cihlar, J., and Goulden, M. L.: Daily canopy photosynthesis model through temporal and spatial scaling

https://doi.org/10.5194/essd-2022-15
Preprint. Discussion started: 4 February 2022

for remote sensing applications, Ecol. Modell., 124, 99–119, https://doi.org/10.1016/S0304-3800(99)00156-8, 1999.

Chevallier, F., Palmer, P. I., Feng, L., Boesch, H., O'Dell, C. W., and Bousquet, P.: Toward robust and consistent regional CO_2 flux estimates from in situ and spaceborne measurements of atmospheric CO_2, Geophys. Res. Lett., 41, 1065–1070, https://doi.org/10.1002/2013GL058772, 2014.

Ciais, P., Bastos, A., Chevallier, F., Lauerwald, R., Poulter, B., Canadell, P., Hugelius, G., Jackson, R. B., Jain, A., Jones, M., Kondo, M., Luijkx, I., Patra, P. K., Peters, W., Pongratz, J., Petrescu, A. M. R., Piao, S., Qiu, C., Von Randow, C., Regnier, P., Saunois, M., Scholes, R., Shvidenko, A., Tian, H., Yang, H., Wang, X., and Zheng, B.: Definitions and methods to estimate regional land carbon fluxes for the second phase of the REgional Carbon Cycle Assessment and Processes Project (RECCAP-2), Geosci. Model Dev. Discuss. [preprint], https://doi.org/10.5194/gmd-2020-259, in review, 2020.

Ciais, P., Borges, A. V., Abril, G., Meybeck, M., Folberth, G., Hauglustaine, D., and Janssens, I. A.: The impact of lateral carbon fluxes on the European carbon balance, Biogeosciences, 5, 1259–1271, https://doi.org/10.5194/bg-5-1259-2008, 2008.

Ciais, P., Reichstein, M., Viovy, N., Granier, A., Ogee, J., Allard, V., Aubinet, M., Buchmann, N., Bernhofer, C., Carrara, A., Chevallier, F., De Noblet, N., Friend, A. D., Friedlingstein, P., Grunwald, T., Heinesch, B., Keronen, P., Knohl, A., Krinner, G., Loustau, D., Manca, G., Matteucci, G., Miglietta, F., Ourcival, J. M., Papale, D., Pilegaard, K., Rambal, S., Seufert, G., Soussana, J. F., Sanz, M. J., Schulze, E. D., Vesala, T., and Valentini, R.: Europewide reduction in primary productivity caused by the heat and drought in 2003, Nature, 437, 529–533, https://doi.org/10.1038/nature03972, 2005.

Ciais, P., Yao, Y., Gasser, T., Baccini, A., Wang, Y., Lauerwald, R., Peng, S., Bastos, A., Li, W., Raymond, P. A., Canadell, J. G., Peters, G. P., Andres, R. J., Chang, J., Yue, C., Dolman, A. J., Haverd, V., Hartmann, J., Laruelle, G., Konings, A. J., King, A. W., Liu, Y., Luyssaert, S., Maignan, F., Patra, P. K., Peregon, A., Regnier, P., Pongratz, J., Poulter, B., Shvidenko, A., Valentini, R., Wang, R., Broquet, G., Yin, Y., Zscheischler, J., Guenet, B., Goll, D. S., Ballantyne, A. P., Yang, H., Qiu, C., and Zhu, D.: Empirical estimates of regional carbon budgets imply reduced global soil heterotrophic respiration, Nat. Sci. Rev., 8(2), nwaa145, https://doi.org/10.1093/nsr/nwaa145, 2021.

Crisp, D., Pollock, H. R., Rosenberg, R., Chapsky, L., Lee, R. A. M., Oyafuso, F. A., Frankenberg, C., O'Dell, C. W., Bruegge, C. J., Doran, G. B., Eldering, A., Fisher, B. M., Fu, D., Gunson, M. R., Mandrake, L., Osterman, G. B., Schwandner, F. M., Sun, K., Taylor, T. E., Wennberg, P. O., and Wunch, D.: The on-orbit performance of the Orbiting Carbon Observatory-2 (OCO-2) instrument and its radiometrically calibrated products, Atmos. Meas. Tech., 10, 59–81, https://doi.org/10.5194/amt-10-59-2017, 2017.

Davis, K. J., Obland, M. D., Lin, B., Lauvaux, T., O'Dell, C., Meadows, B., Browell, E. V., DiGangi, J. P., Sweeney, C., McGill, M. J., Barrick, J. D., Nehrir, A. R., Yang, M. M., Bennett, J. R., Baier, B. C., Roiger, A., Pal, S., Gerken, T., Fried, A., Feng, S., Shrestha, R., Shook, M. A., Chen, G., Campbell, L. J., Barkley, Z. R., and Pauly, R. M.: ACT-America: L3 Merged In Situ Atmospheric Trace Gases and Flask Data, Eastern USA, ORNL DAAC, Oak Ridge, Tennessee, USA, https://doi.org/10.3334/ORNLDAAC/1593, 2018.

Deng, F., Jones, D. B. A., O'Dell, C. W., Nassar, R., and Parazoo, N. C.: Combining GOSAT XCO_2 observations over land and ocean to improve regional CO_2 flux estimates, J. Geophys. Res.-Atmos., 121, 1896–1913, https://doi.org/10.1002/2015JD024157, 2016.

Detmers, R. G., Hasekamp, O., Aben, I., Houweling, S., van Leeuwen, T. T., Butz, A., Landgraf, J., Köhler, P., Guanter, L., and Poulter, B.: Anomalous carbon uptake in Australia as seen by GOSAT, Geophys. Res. Lett., 42, 8177–8184, https://doi.org/10.1002/2015GL065161, 2015.

Doughty, C. E., Metcalfe, D. B., Girardin, C. A. J., Amezquita, F. F., Cabrera, D. G., Huasco, W. H., Silva-Espejo, J. E., Araujo-Murakami, A., da Costa, M. C., Rocha, W., Feldpausch, T. R., Mendoza, A. L. M., da Costa, A. C. L., Meir, P., Phillips, O. L., and Malhi, Y.: Drought impact on forest carbon dynamics and fluxes in Amazonia, Nature, 519, 78–82, https://doi.org/10.1038/nature14213, 2015.

Emmons, L. K., Walters, S., Hess, P. G., Lamarque, J.-F., Pfister, G. G., Fillmore, D., Granier, C., Guenther, A., Kinnison, D., Laepple, T., Orlando, J., Tie, X., Tyndall, G., Wiedinmyer, C., Baughcum, S. L., and Kloster, S.: Description and evaluation of the Model for Ozone and Related chemical Tracers, version 4 (MOZART-4), Geosci. Model Dev., 3, 43–67, https://doi.org/10.5194/gmd-3-43-2010, 2010.

Enting, I. G., and Newsam, G. N.: Atmospheric constituent inversion problems: Implications for baseline monitoring, J. Atmos. Chem., 11, 69– 87, https://doi.org/10.1007/BF00053668, 1990.

Feng, S., Jiang, F., Wang, H., Wang, H., Ju, W., Shen, Y., Zheng, Y., Wu, Z., and Ding, A.: NOx Emission Changes over China during the COVID-19 Epidemic Inferred from Surface NO_2 Observations, Geophys. Res. Lett., 47, e2020GL090080, https://doi.org/10.1029/2020GL090080, 2020.

Frank, D., Reichstein, M., Bahn, M., Thonicke, K., Frank, D., Mahecha, M.D., Smith, P., van der Velde, M., Vicca, S., Babst, F., Beer, C., Buchmann, N., Canadell, J.G., Ciais, P., Cramer, W., Ibrom, A., Miglietta, F., Poulter, B., Rammig, A., Seneviratne, S.I., Walz, A., Wattenbach, M., Zavala, M.A. and Zscheischler, J.: Effects of climate extremes on the terrestrial carbon cycle: concepts, processes and potential future impacts, Glob. Change Biol., 21: 2861-2880. https://doi.org/10.1111/gcb.12916, 2015.

Friedlingstein, P., O'Sullivan, M., Jones, M. W., Andrew, R. M., Hauck, J., Olsen, A., Peters, G. P., Peters, W., Pongratz, J., Sitch, S., Le Quéré, C., Canadell, J. G., Ciais, P., Jackson, R. B., Alin, S., Aragão, L. E. O. C., Arneth, A., Arora, V., Bates, N. R., Becker, M., Benoit-Cattin, A., Bittig, H. C., Bopp, L., Bultan, S., Chandra, N., Chevallier, F., Chini, L. P., Evans, W., Florentie, L., Forster, P. M., Gasser, T., Gehlen, M., Gilfillan, D., Gkritzalis, T., Gregor, L., Gruber, N., Harris, I., Hartung, K., Haverd, V., Houghton, R. A., Ilyina, T., Jain, A. K., Joetzjer, E., Kadono, K., Kato, E., Kitidis, V., Korsbakken, J. I., Landschützer, P., Lefèvre, N., Lenton, A., Lienert, S., Liu, Z., Lombardozzi, D., Marland, G., Metzl, N., Munro, D. R., Nabel, J. E. M. S., Nakaoka, S.-I., Niwa, Y., O'Brien, K., Ono, T., Palmer, P. I., Pierrot, D., Poulter, B., Resplandy, L., Robertson, E., Rödenbeck, C., Schwinger, J., Séférian, R., Skjelvan, I., Smith, A. J. P., Sutton, A. J., Tanhua, T., Tans, P. P., Tian, H., Tilbrook, B., van der Werf, G., Vuichard, N., Walker, A. P., Wanninkhof, R., Watson, A. J., Willis, D., Wiltshire, A. J., Yuan, W., Yue, X., and Zaehle, S.: Global Carbon Budget 2020, Earth Syst. Sci. Data, 12, 3269–3340, https://doi.org/10.5194/essd-12-3269-2020, 2020.

Gahlot, S., Shu, S., Jain, A. K., and Roy, S. B.: Estimating trends and variation of net biome productivity in India for 1980–2012 using a land surface model, Geophys. Res. Lett., 44, 11573–11579. https://doi.org/10.1002/2017GL075777, 2017.

Gasser, T., Crepin, L., Quilcaille, Y., Houghton, R. A., Ciais, P., and Obersteiner, M.: Historical CO_2 emissions from land use and land cover change and their uncertainty, Biogeosciences, 17, 4075–4101, https://doi.org/10.5194/bg-17-4075-2020, 2020.

Gatti, L. V., Gloor, M., Miller, J. B., Doughty, C. E., Malhi, Y., Domingues, L. G., Basso, L. S., Martinewski, A., Correia, C. S. C., Borges, V. F., Freitas, S., Braz, R., Anderson, L. O., Rocha, H., Grace, J., Phillips, O. L., and Lloyd, J.: Drought sensitivity of Amazonian carbon balance revealed by atmospheric measurements, Nature, 506, 76–80, https://doi.org/10.1038/nature12957, 2014.

Gatti, L. V., Correa, C. C. S., Domingues, L. G., Miller, J. B., Gloor, M., Martinewski, A., Basso, L. S., Santana, R., Crispim, S. P., Marani, L., and Neves, R. L.: CO_2 Vertical Profiles on Four Sites over Amazon from 2010 to 2018, PANGAEA, https://doi.org/10.1594/PANGAEA.926834, 2021.

Ghimire, B., Williams, C.A., Collatz, G.J., Vanderhoof, M., Rogan, J., Kulakowski, D. and Masek, J.G.: Large carbon release legacy from bark beetle outbreaks across Western United States, Glob. Change Biol., 21, 3087–3101. https://doi.org/10.1111/gcb.12933, 2015.

Graf, A., Klosterhalfen, A., Arriga, N., Bernhofer, C., Bogena, H., Bornet, F., Brüggemann, N., Brümmer, C., Buchmann, N., Chi, J., Chipeaux, C., Cremonese, E., Cuntz, M., Dušek, J., El-Madany, T. S., Fares, S., Fischer, M., Foltýnová, L., Gharun, M., Ghiasi, S., Gielen, B., Gottschalk, P., Grünwald, T., Heinemann, G., Heinesch, B., Heliasz, M., Holst, J., Hörtnagl, L., Ibrom, A., Ingwersen, J., Jurasinski, G., Klatt, J., Knohl, A., Koebsch, F., Konopka, J., Korkiakoski, M., Kowalska, N., Kremer, P., Kruijt, B., Lafont, S., Léonard, J., De Ligne, A., Longdoz, B., Loustau, D., Magliulo, V., Mammarella, I., Manca, G., Mauder, M., Migliavacca, M., Mölder, M., Neirynck, J., Ney, P., Nilsson, M., Paul-Limoges, E., Peichl, M., Pitacco, A., Poyda, A., Rebmann, C., Roland, M., Sachs, T., Schmidt, M., Schrader, F., Siebicke, L., Šigut, L., Tuittila, E.-S., Varlagin, A., Vendrame, N., Vincke, C., Völksch, I., Weber, S., Wille, C., Wizemann, H.-D., Zeeman, M. and Vereecken, H.: Altered energy partitioning across terrestrial ecosystems in the European drought year 2018, Philos. Trans. R. Soc. B-Biol. Sci., 375, 20190524, https://doi.org/10.1098/rstb.2019.0524, 2020.

Gurney, K. R., Law, R. M., Denning, A. S., Rayner, P. J., Baker, D., Bousquet, P., Bruhwiler, L., Chen, Y.-H., Ciais, P., Fan, S., Fung, I. Y., Gloor, M., Heimann, M., Higuchi, K., John, J., Maki, T., Maksyutov, S., Masarie, K., Peylin, P., Prather, M., Pak, B. C., Randerson, J., Sarmiento, J., Taguchi, S., Takahashi, T., and Yuen, C.-W.: Towards robust regional estimates of CO_2

https://doi.org/10.5194/essd-2022-15
Preprint. Discussion started: 4 February 2022

Open Access Earth System Science Data Discussions

sources and sinks using atmospheric transport models, Nature, 415, 626–630, https://doi.org/10.1038/415626a, 2002.

Gurney, K. R., Law, R. M., Denning, A. S., Rayner, P. J., Baker, D., Bousquet, P., Bruhwiler, L., Chen, Y. H. Ciais, P., Fan, S., Fung, I. Y., Gloor, M., Heimann, M., Higuchi, K., John, J., Kowalczyk, E., Maki, T., Maksyutov, S., Peylin, P., Prather, M., Pak, B. C., Sarmiento, J., Taguchi, S., Takahashi, T., and Yuen, C. W.: Transcom 3 CO_2 Inversion Intercomparison: 1. Annual mean control results and sensitivity to transport and prior flux information, Tellus B, 55, 555–579, https://doi.org/10.1034/j.1600-0560.2003.00049.x, 2003.

Hansis, E., Davis, S. J., and Pongratz, J.: Relevance of methodological choices for accounting of land use change carbon fluxes, Glob. Biogeochem. Cycle, 29, 1230–1246, https://doi.org/10.1002/2014GB004997, 2015.

He, W., Jiang, F., Ju, W., Nguyen, T. N., Fang, M., He, Q., and Zhang, C.: Ensemble Satellite Land Products Deepen the Interpretation of Drought Impacts on Terrestrial Carbon Cycle in Europe Over 2001–2015, 2019 IEEE International Geoscience and Remote Sensing Symposium, pp. 9273–9276, https://doi.org/10.1109/IGARSS.2019.8898928, 2019.

He, W., Ju, W., Schwalm, C., Sippel, S., Wu, X., He, Q., Song, L., Zhang, C., Li, J., Sitch, S., Viovy, N., Friedlingstein, P., and Jain, A.: Terrestrial net carbon uptake over North America in 2011 and 2012, J. Geophys. Res.- Biogeosci., 123(7), 2053– 2071. https://doi.org/10.1029/2018JG004520, 2018.

Houghton, R. A. and Nassikas, A. A.: Global and regional fluxes of carbon from land use and land cover change 1850-2015, Glob. Biogeochem. Cycle, 31, 456–472, https://doi.org/10.1002/2016GB005546, 2017.

Houweling, S., Baker, D., Basu, S., Boesch, H., Butz, A., Chevallier, F., Deng, F., Dlugokencky, E. J., Feng, L., Ganshin, A., Hasekamp, O., Jones, D., Maksyutov, S., Marshall, J., Oda, T., O'Dell, C. W., Oshchepkov, S., Palmer, P. I., Peylin, P., Poussi, Z., Reum, F., Takagi, H., Yoshida, Y., and Zhuravlev, R.: An intercomparison of inverse models for estimating sources and sinks of CO_2 using GOSAT measurements, J. Geophys. Res.-Atmos., 120, 5253–5266, https://doi.org/10.1002/2014JD022962, 2015.

Jacobson, A. R., Schuldt, K. N., Miller, J. B., Oda, T., Tans, P., Andrews, A., Mund, J., Ott, L., Collatz, G. J., Aalto, T., Afshar, S., Aikin, K., Aoki, S., Apadula, F., Baier, B., Bergamaschi, P., Beyersdorf, A., Biraud, S. C., Bollenbacher, A., Bowling, D., Brailsford, G., Abshire, J. B., Chen, G., Chen, H., Chmura, L., Climadat, S., Colomb, A., Conil, S., Cox, A., Cristofanelli, P., Cuevas, E., Curcoll, R., Sloop, C. D., Davis, K., Wekker, S. D., Delmotte, M., DiGangi, J. P., Dlugokencky, E., Ehleringer, J., Elkins, J. W., Emmenegger, L., Fischer, M. L., Forster, G., Frumau, A., Galkowski, M., Gatti, L. V., Gloor, E., Griffis, T., Hammer, S., Haszpra, L., Hatakka, J., Heliasz, M., Hensen, A., Hermanssen, O., Hintsa, E., Holst, J., Jaffe, D., Karion, A., Kawa, S. R., Keeling, R., Keronen, P., Kolari, P., Kominkova, K., Kort, E., Krummel, P., Kubistin, D., Labuschagne, C., Langenfelds, R., Laurent, O., Laurila, T., Lauvaux, T., Law, B., Lee, J., Lehner, I., Leuenberger, M., Levin, I., Levula, J., Lin, J., Lindauer, M., Loh, Z., Lopez, M., Lund Myhre, C., Machida, T., Mammarella, I., Manca, G., Manning, A., Manning, A., Marek, M. V., Marklund, P., Martin, M. Y., Matsueda, H., McKain, K., Meijer, H., Meinhardt, F., Miles, N., Miller, C. E., Mölder, M., Montzka, S., Moore, F., Morgui, J.-A., Morimoto, S., Munger, B., Necki, J., Newman, S., Nichol, S., Niwa, Y., O'Doherty, S., Ottosson-Löfvenius, M., Paplawsky, B., Peischl, J., Peltola, O., Pichon, J.-M., Piper, S., Plass-Dölmer, C., Ramonet, M., Reyes-Sanchez, E., Richardson, S., Riris, H., Ryerson, T., Saito, K., Sargent, M., Sawa, Y., Say, D., Scheeren, B., Schmidt, M., Schmidt, A., Schumacher, M., Shepson, P., Shook, M., Stanley, K., Steinbacher, M., Stephens, B., Sweeney, C., Thoning, K., Torn, M., Turnbull, J., Tørseth, K., Bulk, P. V. D., Laan-Luijkx, I. T. V. D., Dinther, D. V., Vermeulen, A., Viner, B., Vitkova, G., Walker, S., Weyrauch, D., Wofsy, S., Worthy, D., Young, D., and Zimnoch, M.: CarbonTracker CT2019, https://doi.org/10.25925/39m3-6069, 2020.

Jiang, F., Wang, H. M., Chen, J. M., Machida, T., Zhou, L. X., Ju, W. M., Matsueda, H., and Sawa, Y.: Carbon balance of China constrained by CONTRAIL aircraft CO_2 measurements, Atmos. Chem. Phys., 14, 10133–10144. https://doi.org/10.5194/acp-14-1070 10133-2014, 2014.

Jiang, F., Wang, H., Chen, J. M., Ju, W., Tian, X., Feng, S., Li, G., Chen, Z., Zhang, S., Lu, X., Liu, J., Wang, H., Wang, J., He, W., and Wu, M.: Regional CO_2 fluxes from 2010 to 2015 inferred from GOSAT XCO_2 retrievals using a new version of the Global Carbon Assimilation System, Atmos. Chem. Phys., 21, 1963–1985, https://doi.org/10.5194/acp-21-1963-2021, 2021.

Jiang, F., Chen, J. M., Zhou, L. X., Ju, W. M., Zhang, H. F., Machida T., Ciais, P., Peters, W., Wang, H. M., Chen, B. Z., Liu, L. X., Zhang, C. H., Matsueda, H., and Sawa, Y.: A comprehensive estimate of recent carbon sinks in China using both top-down and bottom-up approaches, Sci Rep, 6, https://doi.org/10.1038/srep22130, 2016.

Jung, M., Reichstein, M., and Bondeau, A.: Towards global empirical upscaling of FLUXNET eddy covariance observations: validation of a model tree ensemble approach using a biosphere model, Biogeosciences, 6, 2001–2013, https://doi.org/10.5194/bg-6-2001-2009, 2009.

Koren, G., Van Schaik, E., Araújo, A.C., Boersma, K.F., Gärtner, A., Killaars, L., Kooreman, M.L., Kruijt, B., Van der Laan-Luijkx, I.T., Von Randow, C., Smith, N.E., and Peters, W.: Widespread reduction in sun-induced fluorescence from the Amazon during the 2015/2016 El Niño. Philos. Trans. R. Soc. B-Biol. Sci., 373, 20170408, http://dx.doi.org/10.1098/rstb.2017.0408, 2018.

Kulawik, S. S., Crowell, S., Baker, D., Liu, J., McKain, K., Sweeney, C., Biraud, S. C., Wofsy, S., O'Dell, C. W., Wennberg, P. O., Wunch, D., Roehl, C. M., Deutscher, N. M., Kiel, M., Griffith, D. W. T., Velazco, V. A., Notholt, J., Warneke, T., Petri, C., De Mazière, M., Sha, M. K., Sussmann, R., Rettinger, M., Pollard, D. F., Morino, I., Uchino, O., Hase, F., Feist, D. G., Roche, S., Strong, K., Kivi, R., Iraci, L., Shiomi, K., Dubey, M. K., Sepulveda, E., Rodriguez, O. E. G., Té, Y., Jeseck, P., Heikkinen, P., Dlugokencky, E. J., Gunson, M. R., Eldering, A., Crisp, D., Fisher, B., and Osterman, G. B.: Characterization of OCO-2 and ACOS-GOSAT biases and errors for CO_2 flux estimates, Atmos. Meas. Tech. Discuss. [preprint], https://doi.org/10.5194/amt-2019-257, 2019.

Kuze, A., Suto, H., Nakajima, M., and Hamazaki, T.: Thermal and near infrared sensor for carbon observation Fourier-

https://doi.org/10.5194/essd-2022-15
Preprint. Discussion started: 4 February 2022

transform spectrometer on the Greenhouse Gases Observing Satellite for greenhouse gases monitoring, Appl. Opt., 48, 6716, https://doi.org/10.1364 /AO.48.006716, 2009.

Li, X., Xiao, J., Kimball, J. S., Reichle, R. H., Scott, R. L., Litvak, M. E., Bohrer, G., and Frankenberg, C.: Synergistic use of SMAP and OCO-2 data in assessing the responses of ecosystem productivity to the 2018 U.S. drought, Remote Sens. Environ., 251, 112062, https://doi.org/10.1016/j.rse.2020.112062, 2020.

Liu, J., Baskaran, L., Bowman, K., Schimel, D., Bloom, A. A., Parazoo, N. C., Oda, T., Carroll, D., Menemenlis, D., Joiner, J., Commane, R., Daube, B., Gatti, L. V., McKain, K., Miller, J., Stephens, B. B., Sweeney, C., and Wofsy, S.: Carbon Monitoring System Flux Net Biosphere Exchange 2020 (CMS-Flux NBE 2020), Earth Syst. Sci. Data, 13, 299–330, https://doi.org/10.5194/essd-13-299-2021, 2021.

Liu, J., Bowman, K. W., Lee, M., Henze, D. K., Bousserez, N., Brix, H., James Collatz, G., Menemenlis, D., Ott, L., Pawson, S., and Jones, D.: Carbon monitoring system flux estimation and attribution: impact of ACOS-GOSAT XCO_2 sampling on the inference of terrestrial biospheric sources and sinks, Tellus B, 66, 22486, https://doi.org/10.3402/tellusb.v66.22486, 2014.

Liu, J., Bowman, K. W., Schimel, D. S., Parazoo, N. C., Jiang, Z., Lee, M., Bloom, A. A., Wunch, D., Frankenberg, C., Sun, Y., O'Dell, C. W., Gurney, K. R., Menemenlis, D., Gierach, M., Crisp, D., and Eldering, A.: Contrasting carbon cycle responses of the tropical continents to the 2015–2016 El Niño, Science, 358, eaam5690, https://doi.org/10.1126/science.aam5690, 2017.

Liu, J., Bowman, K., Parazoo, N. C., Bloom, A A., Wunch, D., Jiang, Z., Gurney, K. R., and Schimel, D.: Detecting drought impact on terrestrial biosphere carbon fluxes over contiguous US with satellite observations, Environ. Res. Lett., 13(9), 095003, https://doi.org/10.1088/1748-9326/aad5ef, 2018.

Machida, T., Matsueda, H., Sawa, Y., Nakagawa, Y., Hirotani, K., Kondo, N., Goto, K., Ishikawa, K., Nakazawa, T., and Ogawa, T.: Worldwide measurements of atmospheric CO_2 and other trace gas species using commercial airlines, J. Atmos. Ocean. Technol., 25, 1744–1754, https://doi.org/10.1175/2008JTECHA1082.1, 2008.

Maksyutov, S., Takagi, H., Valsala, V. K., Saito, M., Oda, T., Saeki, T., Belikov, D. A., Saito, R., Ito, A., Yo-shida, Y., Morino, I., Uchino, O., Andres, R. J., and Yokota, T.: Regional CO_2 flux estimates for 2009–2010 based on GOSAT and ground- based CO_2 observations, Atmos. Chem. Phys., 13, 9351–9373, https://doi.org/10.5194/acp-13-9351-2013, 2013.

Machida, T., Ishijima, K., Niwa, Y., Tsuboi, K., Sawa, Y., Matsueda, H., and Sasakawa, M.: Atmospheric CO_2 mole fraction data of CONTRAIL-CME, ver.2020.1.0, Center for Global Environmental Research, NIES, https://doi.org/10.17595/20180208.001, (Reference date: 2021/02/05), 2018.

Matsueda, H., Machida, T., Sawa, Y., and Niwa, Y.: Long-term change of CO_2 latitudinal distribution in the upper troposphere. Geophys. Res. Lett., 42, 2508–2514. http://doi.org/10.1002/2014GL062768, 2015.

Matsueda, H., Machida, T., Sawa, Y., Nakagawa, Y., Hirotani, K., Ikeda, H., Kondo, N., and Goto, K.: Evaluation of atmospheric CO_2 measurements from new flask air sampling of JAL airliner observations, Pap. Meteorol. Geophys., 59, 1–17, http://doi.org/10.2467/mripapers.59.1, 2008.

Mu, M., Randerson, J. T., van der Werf, G. R., Giglio, L., Kasibhatla, P., Morton, D., Collatz, G. J., Defries, R. S., Hyer, E. J., Prins, E. M., Griffith, D. W. T., Wunch, D., Toon, G. C., Sherlock, V. and Wennberg, P. O.: Daily and 3-hourly variability in global fire emissions and consequences for atmospheric model predictions of carbon monoxide, J. Geophys. Res.-Atmos., 116(D24), https://doi.org/10.1029/2011JD016245, 2011.

Nayak, R. K., Patel, N. R., and Dadhwal, V. K.: Spatio-temporal variability of net ecosystem productivity over India and its relationship to climatic variables. Environ. Earth Sci., 74, 1743–1753. https://doi.org/10.1007/s12665-015-4182-4, 2015.

Niwa, Y., Machida, T., Sawa, Y., Matsueda, H., Schuck, T. J., Brenninkmeijer, C. A. M., Imasu, R., and Satoh, M.: Imposing strong constraints on tropical terrestrial CO_2 fluxes using passenger aircraft based measurements. J. Geophys. Res., 117, D11303, https://doi.org/10.1029/2012JD017474, 2012.

Oda, T., Maksyutov, S., and Andres, R. J.: The Open-source Data Inventory for Anthropogenic CO2, version 2016 (ODIAC2016): a global monthly fossil fuel CO_2 gridded emissions data product for tracer transport simulations and surface flux inversions, Earth Syst. Sci. Data, 10, 87–107, https://doi.org/10.5194/essd-10-87-2018, 2018.

O'Dell, C. W., Eldering, A., Wennberg, P. O., Crisp, D., Gunson, M. R., Fisher, B., Frankenberg, C., Kiel, M., Lindqvist, H., Mandrake, L., Merrelli, A., Natraj, V., Nelson, R. R., Osterman, G. B., Payne, V. H., Taylor, T. E., Wunch, D., Drouin, B. J., Oyafuso, F., Chang, A., McDuffie, J., Smyth, M., Baker, D. F., Basu, S., Chevallier, F., Crowell, S. M. R., Feng, L., Palmer, P. I., Dubey, M., García, O. E., Griffith, D. W. T., Hase, F., Iraci, L. T., Kivi, R., Morino, I., Notholt, J., Ohyama, H., Petri, C., Roehl, C. M., Sha, M. K., Strong, K., Sussmann, R., Te, Y., Uchino, O., and Velazco, V. A.: Improved retrievals of carbon dioxide from Orbiting Carbon Observatory-2 with the version 8 ACOS algorithm, Atmos. Meas. Tech., 11, 6539–6576, https://doi.org/10.5194/amt-11-6539-2018, 2018.

Otto, F. E. L., Massey, N., van Oldenborgh, G. J., Jones, R. G., and Allen, M. R.: Reconciling two approaches to attribution of the 2010 Russian heat wave, Geophys. Res. Lett., 39, L04702, https://doi.org/10.1029/2011GL050422, 2012.

Palmer, P. I., Feng, L., Baker, D., Chevallier, F., Bösch, H., and Somkuti, P.: Net carbon emissions from African biosphere dominate pan-tropical atmospheric CO_2 signal, Nat. Commun., 10, 3344, https://doi.org/10.1038/s41467-019-11097-w, 2019.

Patra, P. K., Canadell, J. G., Houghton, R. A., Piao, S. L., Oh, N.-H., Ciais, P., Manjunath, K. R., Chhabra, A., Wang, T., Bhattacharya, T., Bousquet, P., Hartman, J., Ito, A., Mayorga, E., Niwa, Y., Raymond, P. A., Sarma, V. V. S. S., and Lasco, R.: The carbon budget of South Asia, Biogeosciences, 10, 513–527, https://doi.org/10.5194/bg-10-513-2013, 2013.

Peylin, P., Law, R. M., Gurney, K. R., Chevallier, F., Jacobson, A. R., Maki, T., Niwa, Y., Patra, P. K., Pe-ters, W., Rayner, P. J., Rödenbeck, C., van der Laan-Luijkx, I. T., and Zhang, X.: Global atmospheric carbon budget: results from an ensemble of atmospheric CO2 inversions, Biogeosciences, 10, 6699–6720, https://doi.org/10.5194/bg-10-6699-2013, 2013.

https://doi.org/10.5194/essd-2022-15
Preprint. Discussion started: 4 February 2022

Phillips, O. L., Aragão, L., Lewis, S. L., Fisher, J. B., Lloyd, J., López-González, G., Malhi, Y., Monteagudo, A., Peacock, J., Quesada, C. A., van der Heijden, G., Almeida, S., Amaral, I., Arroyo, L., Aymard, G., Baker, T. R., Bánki, O., Blanc, L., Bonal, D., Brando, P., Chave, J., de Oliveira, A. C. A., Cardozo, N. D., Czimczik, C. I., Feldpausch, T. R., Freitas, M. A., Gloor, E., Higuchi, N., Jiménez, E., Lloyd, G., Meir, P., Mendoza, C., Morel, A., Neill, D. A., Nepstad, D., Patiño, S., Peñuela, M. C., Prieto, A., Ramírez, F., Schwarz, M., Silva, J., Silveira, M., Thomas, A. S., ter Steege, H., Stropp, J., Vásquez, R., Zelazowski, P., Dávila, E. A., Andelman, S., Andrade, A., Chao, K. J., Erwin, T., Di Fiore, A., Honorio, E., Keeling, H., Killeen, T. J., Laurance, W. F., Cruz, A. P., Pitman, N. C. A., Vargas, P. N., Ramírez-Angulo, H., Rudas, A., Salamao, R., Silva, N., Terborgh, J., and Torres-Lezama, A.: Drought sensitivity of the Amazon forest, Science, 323, 1344–1347, https://doi.org/10.1126/science.1164033, 2009.

Piao, S., Wang, X., Wang, K., Li, X., Bastos, A., Canadell, J. G., Ciais, P., Friedlingstein, P., and Sitch, S.: Interannual variation of terrestrial carbon cycle: Issues and perspectives, Glob Change Biol., 26, 300– 318, https://doi.org/10.1111/gcb.14884, 2020.

Quansah, E., Mauder, M., Balogun, A. A., Amekudzi, L. K., Hingerl, L., Bliefernicht, J., and Kunstmann, H.: Carbon dioxide fluxes from contrasting ecosystems in the Sudanian Savanna in West Africa, Carbon Balanc. Manag., 10, 1, https://doi.org/10.1186/s13021-014-0011-4, 2015.

Raczka, B., Hoar, T. J., Duarte, H. F., Fox, A. M., Anderson, J. L., Bowling, D. R., and Lin, J. C.: Improving CLM5.0 biomass and carbon exchange across the Western United States using a data assimilation system, J. Adv. Model. Earth Syst., 13, e2020MS002421, https://doi.org/10.1029/2020MS002421, 2021.

Ramo, R., Roteta, E., Bistinas, I., van Wees, D., Bastarrika, A., Chuvieco, E., and van der Werf, G. R.: African burned area and fire carbon emissions are strongly impacted by small fires undetected by coarse resolution satellite data, Proc. Natl. Acad. Sci. U. S. A., 118(9), e2011160118, https://doi.org/10.1073/pnas.2011160118, 2021.

Räsänen, M., Aurela, M., Vakkari, V., Beukes, J. P., Tuovinen, J.-P., Van Zyl, P. G., Josipovic, M., Venter, A. D., Jaars, K., Siebert, S. J., Laurila, T., Rinne, J., and Laakso, L.: Carbon balance of a grazed savanna grassland ecosystem in South Africa, Biogeosciences, 14, 1039–1054, https://doi.org/10.5194/bg-14-1039-2017, 2017.

Reichstein, M., Bahn, M., Ciais, P., Frank, D., Mahecha, M. D., Seneviratne, S. I., Zscheischler, J., Beer, C., Buchmann, N., Frank, D. C., Papale, D., Rammig, A., Smith, P., Thonicke, K., van der Velde, M., Vicca, S., Walz, A., and Wattenbach, M.: Climate extremes and the carbon cycle, Nature, 500, 287–295, https://doi.org/10.1038/nature12350, 2013.

Rödenbeck, C., Houweling, S., Gloor, M., and Heimann, M.: CO_2 flux history 1982–2001 inferred from atmospheric data using a global inversion of atmospheric transport, Atmos. Chem. Phys., 3, 1919–1964, https://doi.org/10.5194/acp-3-1919-2003, 2003.

Saeki, T., Maksyutov, S., Saito, M., Valsala, V., Oda, T., An- dres, R. J., Belikov, D., Tans, P., Dlugokencky, E., Yoshida, Y., Morino, I., Uchino, O., and Yokota, T.: Inverse modeling of CO_2 fluxes using GOSAT data and multi-year ground-based observations, SOLA, 9, 45–50, https://doi.org/10.2151/sola.2013-011, 2013.

Schuldt, K., Mund, J., Luijkx, I. T., Jacobson, A. R., Aalto, T., Abshire, J. B., Aikin, K., Andrews, A., Aoki, S., Apadula, F., Baier, B., Bakwin, P., Bartyzel, J., Bentz, G., Bergamaschi, P., Beyersdorf, A., Biermann, T., Biraud, S. C., Bowling, D., Brailsford, G., Chen, G., Chen, H., Chmura, L., Clark, S., Climadat, S., Colomb, A., Commane, R., Conil, S., Cox, A., Cristofanelli, P., Cuevas, E., Curcoll, R., Daube, B., Davis, K., De Mazière, M., De Wekker, S., Coletta, J. D., Delmotte, M., DiGangi, J. P., Dlugokencky, E., Elkins, J. W., Emmenegger, L., Fischer, M. L., Forster, G., Frumau, A., Galkowski, M., Gatti, L. V., Gheusi, F., Gloor, E., Gomez-Trueba, V., Goto, D., Griffis, T., Hammer, S., Hanson, C., Haszpra, L., Hatakka, J., Heliasz, M., Hensen, A., Hermanssen, O., Hintsa, E., Holst, J., Jaffe, D., Joubert, W., Karion, A., Kawa, S. R., Keeling, R., Keronen, P., Kolari, P., Kominkova, K., Kort, E., Krummel, P., Kubistin, D., Labuschagne, C., Langenfelds, R., Laurent, O., Laurila, T., Lauvaux, T., Law, B., Lee, J., Lehner, I., Leuenberger, M., Levin, I., Levula, J., Lin, J., Lindauer, M., Loh, Z., Lopez, M., Machida, T., Mammarella, I., Manca, G., Manning, A., Manning, A., Marek, M. V., Martin, M. Y., Matsueda, H., McKain, K., Meijer, H., Meinhardt, F., Merchant, L., Mihalopoulos, N., Miles, N., Miller, J. B., Miller, C. E., Mitchell, L., Montzka, S., Moore, F., Morgan, E., Morgui, J.-A., Morimoto, S., Munger, B., Myhre, C. L., Mölder, M., Müller-Williams, J., Necki, J., Newman, S., Nichol, S., Niwa, Y., O'Doherty, S., Paplawsky, B., Peischl, J., Peltola, O., Pichon, J. M., Piper, S., Plass-Duelmer, C., Ramonet, M., Ramos, R., Reyes-Sanchez, E., Richardson, S., Riris, H., Rivas, P. P., Ryerson, T., Saito, K., Sargent, M., Sawa, Y., Say, D., Scheeren, B., Schmidt, M., Schumacher, M., Sha, M. K., Shepson, P., Shook, M., Sloop, C. D., Smith, P., Steinbacher, M., Stephens, B., Sweeney, C., Tans, P., Thoning, K., Torn, M., Trisolino, P., Turnbull, J., Tørseth, K., Vermeulen, A., Viner, B., Vitkova, G., Walker, S., Weyrauch, D., Wofsy, S., Worthy, D., Young, D., Zimnoch, M., van Dinther, D., and van den Bulk P.: Multi-laboratory compilation of atmospheric carbon dioxide data for the period 1957-2019, obspack_co2_1_GLOBALVIEWplus_v6.0_2020-09-11, NOAA Earth System Research Laboratory, Global Monitoring Laboratory, https://doi.org/10.25925/20200903, 2020.

Sitch, S., Friedlingstein, P., Gruber, N., Jones, S. D., Murray-Tortarolo, G., Ahlström, A., Doney, S. C., Graven, H., Heinze, C., Huntingford, C., Levis, S., Levy, P. E., Lomas, M., Poulter, B., Viovy, N., Zaehle, S., Zeng, N., Arneth, A., Bonan, G., Bopp, L., Canadell, J. G., Chevallier, F., Ciais, P., Ellis, R., Gloor, M., Peylin, P., Piao, S. L., Le Quéré, C., Smith, B., Zhu, Z., and Myneni, R.: Recent trends and drivers of regional sources and sinks of carbon dioxide, Biogeosciences, 12, 653–679, https://doi.org/10.5194/bg-12-653-2015, 2015.

Sleeter, B. M., Liu J., Daniel, C., Rayfield, B., Sherba, J., Hawbaker, T. J., Zhu, Z., Selmants, P. C., and Loveland, T.R.: Effects of contemporary land-use and land-cover change on the carbon balance of terrestrial ecosystems in the United States, Environ. Res. Lett., 13, 045006, https://doi.org/10.1088/1748-9326/aab540, 2018.

Stephens, B., Bent, J., Watt, A., Keeling, R., Morgan, E., and Afshar, S.: ORCAS Airborne Oxygen Instrument. Version 1.0. UCAR/NCAR – Earth Observing Laboratory, https://doi.org/10.5065/D6N29VC6, 2017.

Swathi, P. S., Indira, N. K., and Ramonet M.: Estimation of Carbon dioxide fluxes between land, ocean and atmosphere during 2006-2011 with a 4-D variational assimilation scheme and special reference to Asia, Climate Change and Green Chemistry of CO_2 sequestration, 289–310 (pages), Eds. Goel, M., Satyanarayana, T., and Agrawal, D. P., Springer-Nature Pte Ltd, Singapore, https://doi.org/10.1007/978-981-16-0029-6_17, 2021.

Takagi, H., Saeki, T., Oda, T., Saito, M., Valsala, V., Belikov, D., Saito, R., Yoshida, Y., Morino, I., Uchino, O., Andres, R. J., Yokota, T., and Maksyutov, S.: On the Benefit of GOSAT Observations to the Estimation of Regional CO_2 Fluxes, SOLA, 7, 161-164, https://doi.org/10.2151/sola.2011-041, 2011.

Takahashi, T., Sutherland, S. C., Wanninkhof, R., Sweeney, C., Feely, R. A., Chipman, D. W., Hales, B., Friederich, G., Chavez, F., Sabine, C., Watson, A., Bakker, D. C. E., Schuster, U., Metzl, N., Yoshikawa-Inoue, H., Ishii, M., Midorikawa, T., Nojiri, Y., Körtzinger, A., Steinhoff, T., Hoppema, M., Olafsson, J., Arnarson, T. S., Tilbrook, B., Johannessen, T., Olsen, A., Bellerby, R., Wong, C. S., Delille, B., Bates, N. R., and de Baar, H. J. W.: Climatological mean and decadal change in surface ocean pCO_2, and net sea-air CO_2 flux over the global oceans. Deep-Sea Res. Part II-Top. Stud. Oceanogr., 56 (8-10), 554-577, https://doi.org/10.1016/j.dsr2.2008.12.009, 2009.

Taylor, T. E., O'Dell, C. W., Crisp, D., Kuze, A., Lindqvist, H., Wennberg, P. O., Chatterjee, A., Gunson, M., Eldering, A., Fisher, B., Kiel, M., Nelson, R. R., Merrelli, A., Osterman, G., Chevallier, F., Palmer, P. I., Feng, L., Deutscher, N. M., Dubey, M. K., Feist, D. G., Garcia, O. E., Griffith, D., Hase, F., Iraci, L. T., Kivi, R., Liu, C., De Mazière, M., Morino, I., Notholt, J., Oh, Y.-S., Ohyama, H., Pollard, D. F., Rettinger, M., Roehl, C. M., Schneider, M., Sha, M. K., Shiomi, K., Strong, K., Sussmann, R., Té, Y., Velazco, V. A., Vrekoussis, M., Warneke, T., and Wunch, D.: An eleven year record of XCO_2 estimates derived from GOSAT measurements using the NASA ACOS version 9 retrieval algorithm, Earth Syst. Sci. Data Discuss. [preprint], https://doi.org/10.5194/essd-2021-247, in review, 2021.

Thompson, R. L., Patra, P. K., Chevallier, F., Maksyutov, S., Law, R. M., Ziehn, T., van der Laan-Luijkx, I. T., Peters, W., Ganshin, A., Zhuravlev, R., Maki, T., Nakamura, T., Shirai, T., Ishizawa, M., Saeki, T., Machida, T., Poulter, B., Canadell, J. G., and Ciais, P.: Top–down assessment of the Asian carbon budget since the mid 1990s, Nat. Commun., 7(1), 1–10, https://doi.org/10.1038/ncomms10724, 2016.

Tsuboi, K., Matsueda, H., Sawa, Y., Niwa, Y., Nakamura, M., Kuboike, D., Saito, K., Ohmori, H., Iwatsubo, S., Nishi, H., Hanamiya, Y., Tsuji, K., and Baba, Y.: Evaluation of a new JMA aircraft flask sampling system and laboratory trace gas analysis system, Atmos. Meas. Tech., 6, 1257–1270, https://doi.org/10.5194/amt-6-1257-2013, 2013.

Valentini, R., Arneth, A., Bombelli, A., Castaldi, S., Cazzolla Gatti, R., Chevallier, F., Ciais, P., Grieco, E., Hartmann, J., Henry, M., Houghton, R. A., Jung, M., Kutsch, W. L., Malhi, Y., Mayorga, E., Merbold, L., Murray-Tortarolo, G., Papale, D., Peylin, P., Poulter, B., Raymond, P. A., Santini, M., Sitch, S., Vaglio Laurin, G., van der Werf, G. R., Williams, C. A., and Scholes, R. J.: A full greenhouse gases budget of Africa: synthesis, uncertainties, and vulnerabilities, Biogeosciences, 11, 381–407,

https://doi.org/10.5194/essd-2022-15
Preprint. Discussion started: 4 February 2022

https://doi.org/10.5194/bg-11-381-2014, 2014.

van der Laan-Luijkx, I. T., van der Velde, I. R., Krol, M. C., Gatti, L. V., Domingues, L. G., Correia, C. S. C., Miller, J. B., Gloor, M., van Leeuwen, T. T., Kaiser, J. W., Wiedinmyer, C., Basu, S., Clerbaux, C., and Peters, W.: Response of the Amazon carbon balance to the 2010 drought derived with CarbonTracker South America, Glob. Biogeochem. Cycle, 29, 1092–1108, https://doi.org/10.1002/2014GB005082, 2015.

van der Werf, G. R., Randerson, J. T., Giglio, L., van Leeuwen, T. T., Chen, Y., Rogers, B. M., Mu, M., van Marle, M. J. E., Morton, D. C., Collatz, G. J., Yokelson, R. J., and Kasibhatla, P. S.: Global fire emissions estimates during 1997–2016, Earth Syst. Sci. Data, 9, 697-720, https://doi.org/10.5194/essd-9-697-2017, 2017.

Veenendaal ME, Kolle O, and Lloyd J: Seasonal variation in energy fluxes and carbon dioxide exchange for a broad leaved semi-arid savanna (Mopane woodland) in Southern Africa, Glob. Change Biol., 10(3), 318–328, https://doi.org/10.1111/j.1365-2486.2003.00699.x, 2004.

Wang, H., Jiang, F., Wang, J., Ju, W. M., and Chen, J. M.: Terrestrial ecosystem carbon flux estimated using GOSAT and OCO-2 XCO_2 retrievals, Atmos. Chem. Phys., 19, 12067–12082, https://doi.org/10.5194/acp-19-12067-2019, 2019.

Wang, J., Jiang, F., Wang, H., Qiu, B., Wu, M. S., He, W., Ju, W. M., Zhang, Y. G., Chen, J. M., and Zhou, Y. L.: Constraining global terrestrial gross primary productivity in a global carbon assimilation system with OCO-2 chlorophyll fluorescence data, Agric. For. Meteorol., 304–305, 108424, https://doi.org/10.1016/j.agrformet.2021.108424, 2021a.

Wang, J., Wang, M. R., Kim, J. S., Joiner, J., Zeng, N., Jiang, F., Wang, H., He, W., Wu, M. S., Chen, T. X., Ju, W.M., and Chen, J.M.: Modulation of land photosynthesis by the Indian Ocean Dipole: satellite-based observations and CMIP6 future projections, Earth's Future, https://doi.org/10.1029/2020EF001942, 2021b.

Wang, J., Zeng, N., Wang, M. R., Jiang, F., Chen, J. M., Friedlingstein, P., Jain, A. K., Jiang, Z. Q., Ju, W. M., Lienert, S., Nabel, J., Sitch, S., Viovy, N., Wang, H. M., and Wiltshire, A. J.: Contrasting interannual atmospheric CO_2 variabilities and their terrestrial mechanisms for two types of El Niños, Atmos. Chem. Phys., 18(14): 10333 – 10345, https://doi.org/10.5194/acp-18-10333-2018, 2018.

Wang, S., Zhang, Y., Ju, W, Porcar-Castell, A., Ye, S., Zhang, Z., Brummer, C., Urbaniak, M., Mammarella, I., Juszczak, R., and Boersma, K. F.: Warmer spring alleviated the impacts of 2018 European summer heatwave and drought on vegetation photosynthesis, Agric. For. Meteorol., 295, 108195, https://doi.org/10.1016/j.agrformet.2020.108195, 2020.

Whitaker, J. S., and Hamill, T. M.: Ensemble data assimilation without perturbed observations. Mon. Weather Rev., 130(7), 1913-1924. https://10.1175/1520-0493(2002)130<1913:Edawpo>2.0.Co;2, 2002.

Wofsy, S. C., Afshar, S., Allen, H. M., Apel, E., Asher, E. C., Barletta, B., Bent, J., Bian, H., Biggs, B. C., Blake, D. R., and Blake, N.: ATom: Merged Atmospheric Chemistry, Trace Gases, and Aerosols, ORNL DAAC, Oak Ridge, Tennessee, USA, https://doi.org/10.3334/ORNLDAAC/1581, 2018.

https://doi.org/10.5194/essd-2022-15
Preprint. Discussion started: 4 February 2022

Wofsy, S. C.: HIAPER Pole-to-Pole Observations (HIPPO): Fine-grained, global-scale measurements of climatically important atmospheric gases and aerosols, Philos. T. R. Soc. A, 369, 2073–2086, https://doi.org/10.1098/rsta.2010.0313, 2011.

Wolf, S., Keenan, T. F., Fisher, J. B., Baldocchi, D. D., Desai, A. R., Richardson, A. D., Scott, R. L., Law, B. E., Litvak, M. E., Brunsell, N. A., Peters, W., and van der Laan-Luijkx, I. T.: Warm spring reduced carbon cycle impact of the 2012 US summer drought, Proc. Natl. Acad. Sci. U. S. A., 113 (21), 5880–5885, https://doi.org/10.1073/pnas.1519620113, 2016.

Zeng, J., Matsunaga, T., Tan, Z. H., Saigusa, N., Shirai, T., Tang, Y., Peng, S., and Fukuda. Y.: Global terrestrial carbon fluxes of 1999–2019 estimated by upscaling eddy covariance data with a random forest. Sci. Data, 7, 313, https://doi.org/10.1038/s41597-020-00653-5, 2020.

Zhao, M. S., and Running, S. W.: Drought-Induced Reduction in Global Terrestrial Net Primary Production from 2000 Through 2009, Science, 329, 940-943, https://doi.org/10.1126/science.1192666, 2010.

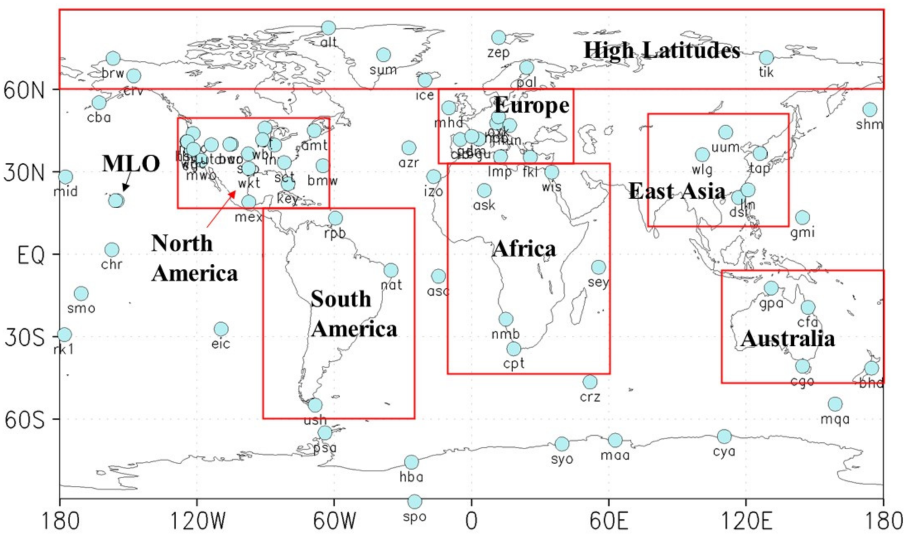

Figure 1: Distributions of the surface flask observation sites used in this study.

https://doi.org/10.5194/essd-2022-15
Preprint. Discussion started: 4 February 2022

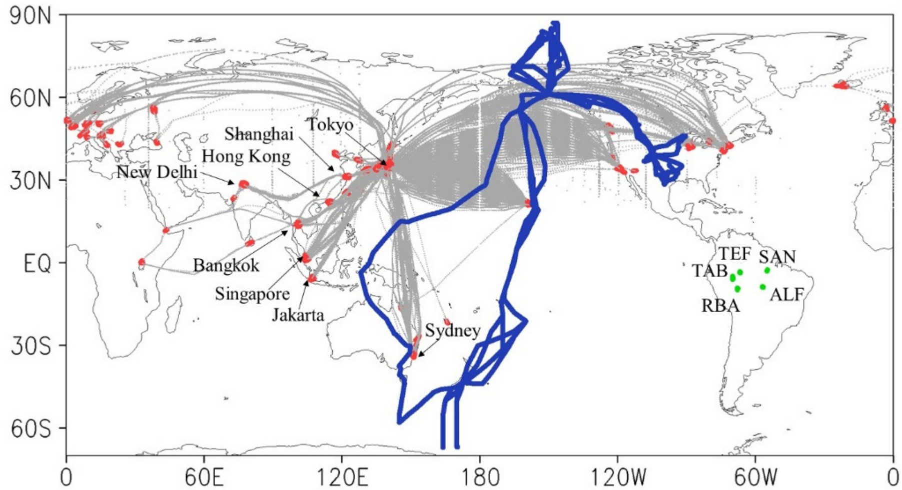

865 **Figure 2: Locations of aircraft observations (red and gray, observations of the CONTRAIL project, in while red marks show observations below 6 km; dark blue, observations of the HIPPO project; green, data of the CARBAM project).**

https://doi.org/10.5194/essd-2022-15
Preprint. Discussion started: 4 February 2022

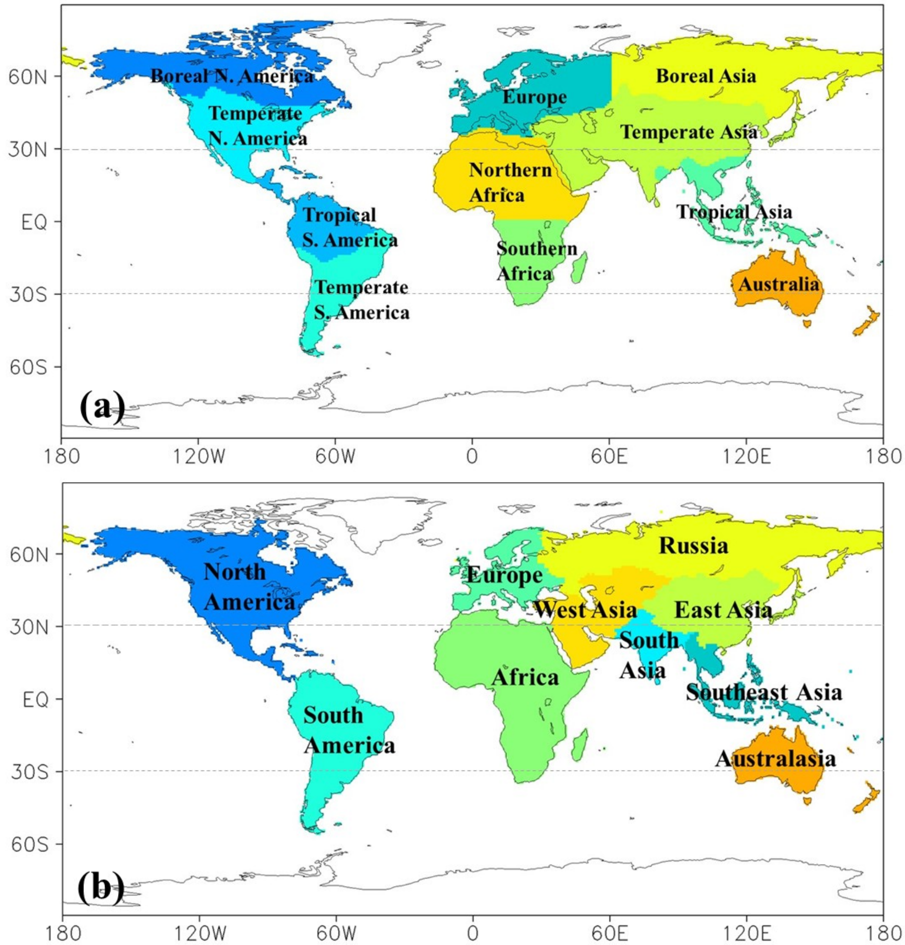

Figure 3: Map of regional masks used in calculating regional fluxes, (a) the TRANSCOM 3 region, (b) the RECCAP2 region.

870

https://doi.org/10.5194/essd-2022-15
Preprint. Discussion started: 4 February 2022

Open Access Earth System Science Data Discussions

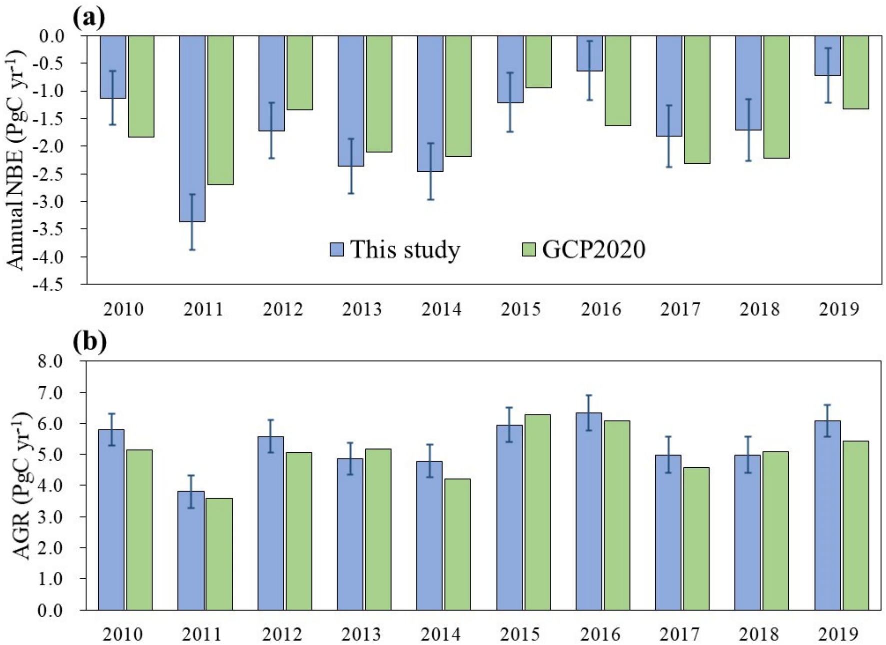

Figure 4: Comparisons between this study and GCP2020 for (a) NBE and (b) Atmospheric Growth Rate (AGR), the NBE of GCP2020 is the sum of land sink and land-use change carbon emission, the AGR of this study is the Net Flux as listed in Table 1.

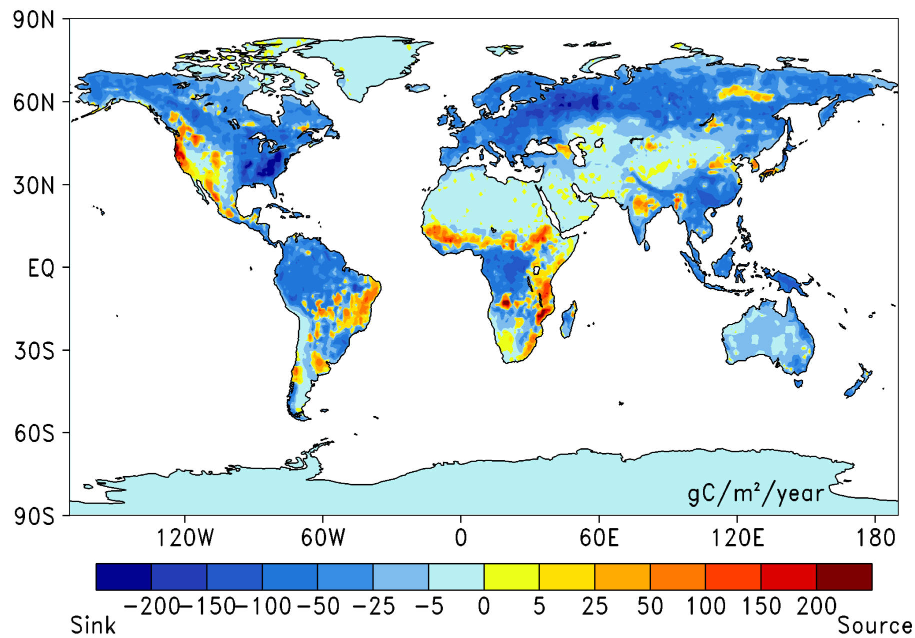

Figure 5: Global distribution of mean annual NEE during 2010-2019.

https://doi.org/10.5194/essd-2022-15
Preprint. Discussion started: 4 February 2022

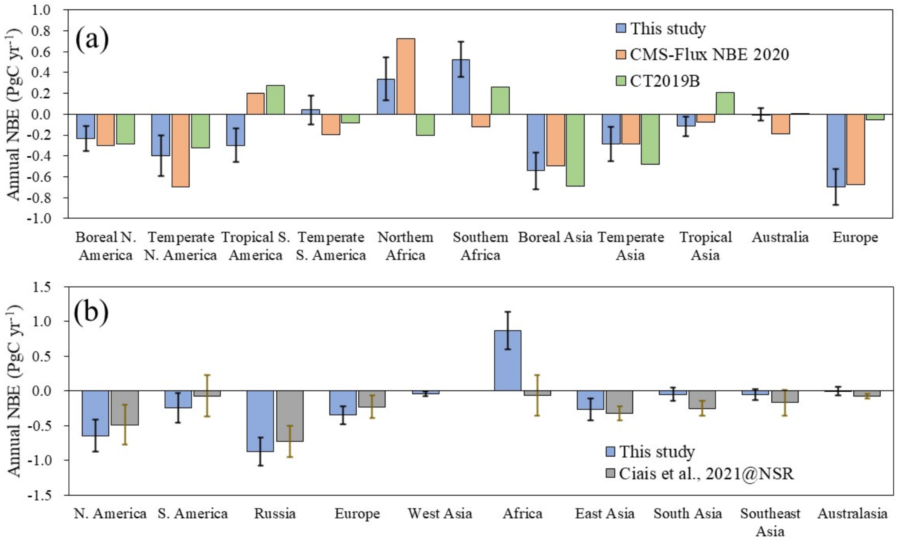

Figure 6: 2010-2019 averaged regional NBE in a) the TRANSCOM 3 regions, and b) the RECCAP2 regions, both CMS-Flux NBE 2020 and CT2019B are averaged from 2010 to 2018, the result of Ciais et al. (2021) is a bottom-up estimate, which is for the period of 2000-2009.

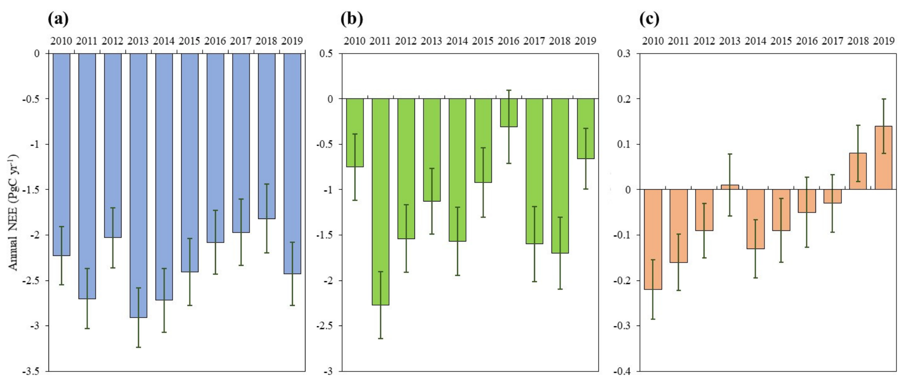

Figure 7: Interannual variations of annual NEE of different latitudes (a, northern mid-high latitudes; b, low latitudes; c, southern middle latitudes).

https://doi.org/10.5194/essd-2022-15
Preprint. Discussion started: 4 February 2022

Open Access Earth System Science Data Discussions

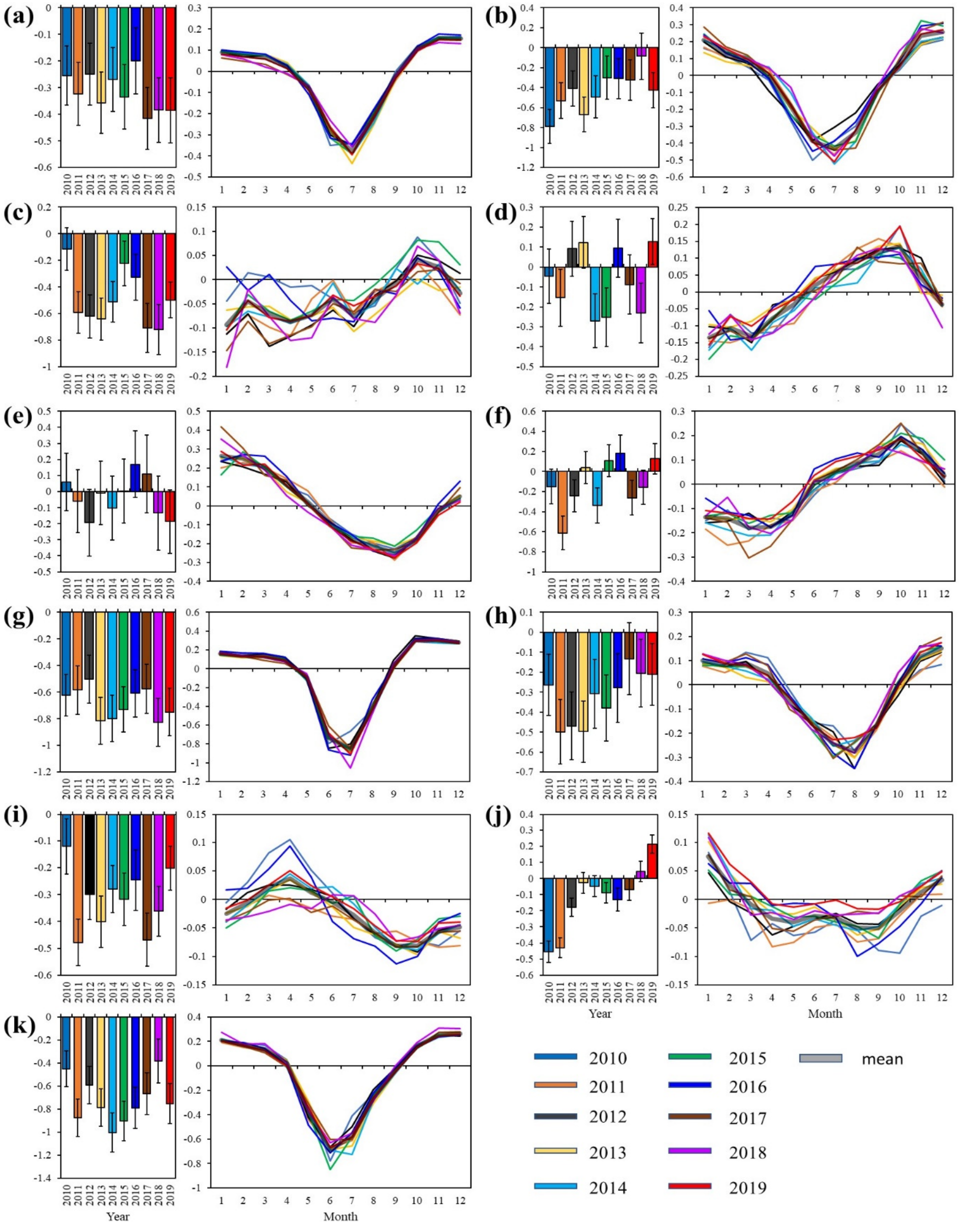

885

Figure 8: Interannual variations of the annual (unit: PgC yr-1) and monthly (unit: unit: PgC month-1) NEE in the 11 TRANSCOM regions (a, boreal N. America; b, temperate N. America; c, tropical S. America; d, temperate S. America; e, northern Africa; f, southern Africa; g, boreal Asia; h, temperate Asia; i, tropical Asia; j, Australia; k, Europe).

https://doi.org/10.5194/essd-2022-15
Preprint. Discussion started: 4 February 2022

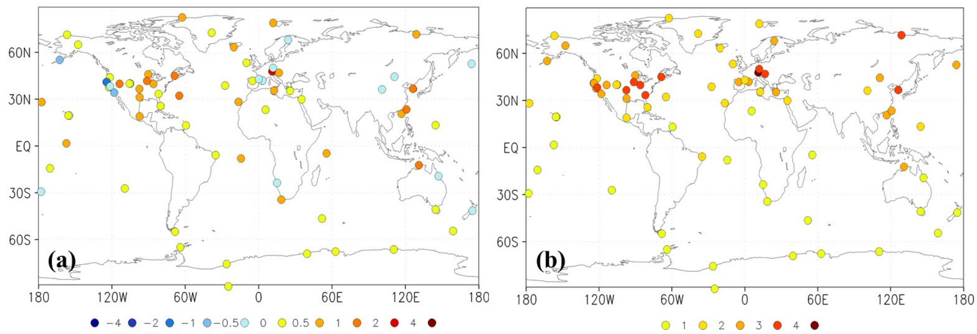

Figure 9: Spatial distributions of BIAS and MAE of each site (unit: ppm)

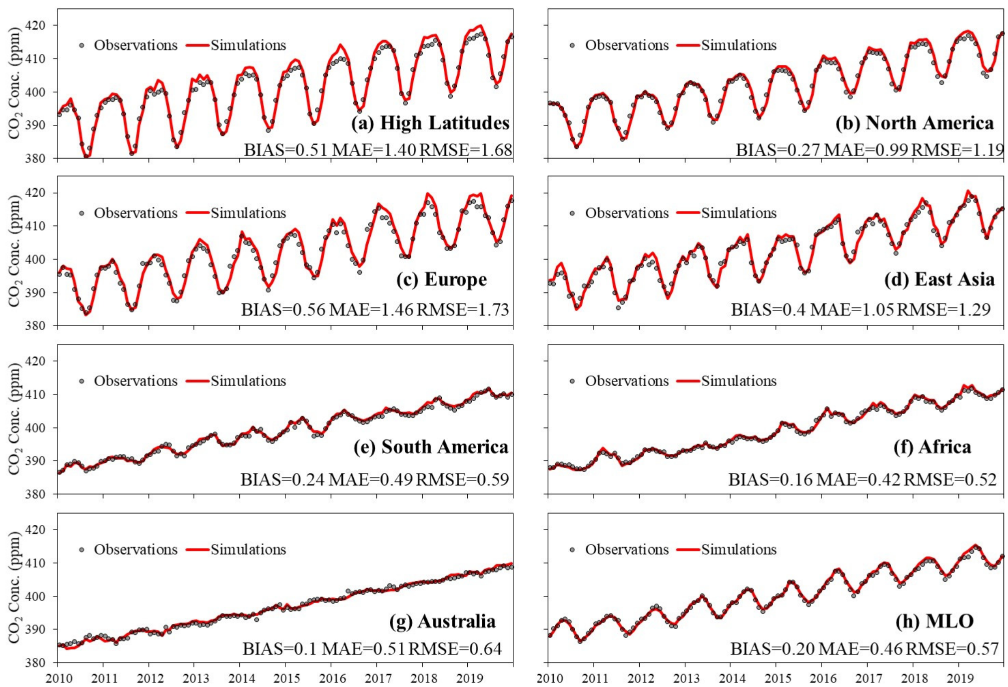

Figure 10: Time series of monthly averaged observations and simulations in the 7 regions and MLO site.

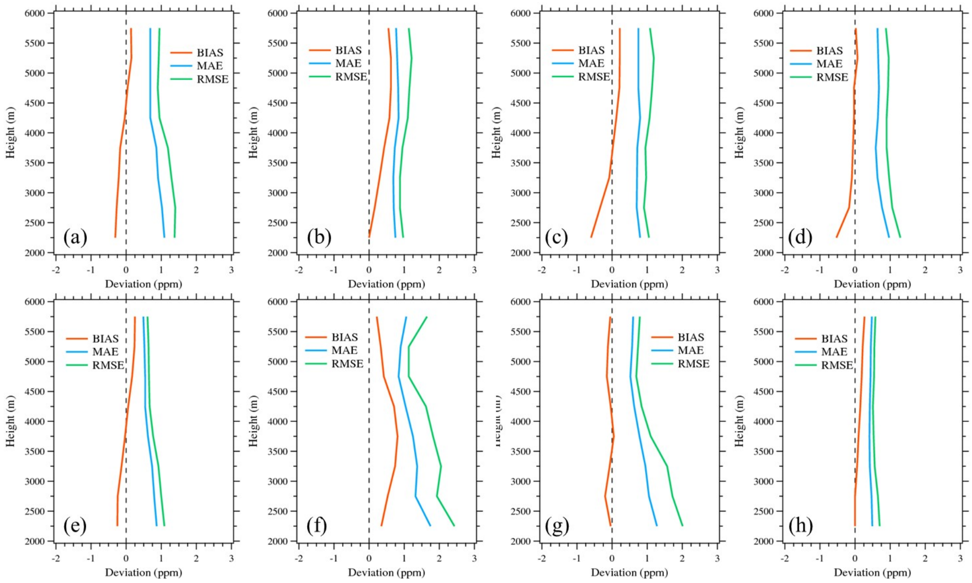

Figure 11: Statistical results for monthly mean profiles in the 8 Asia-Pacific cities (a, Hong Kong; b, Bangkok; c, Singapore; d, Jakarta; d, Tokyo; f, Shanghai; g, New Delhi; h, Sydney).

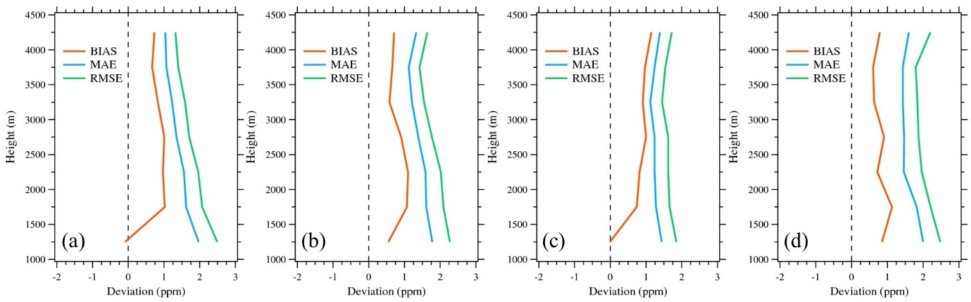

Figure 12: Statistical results at different heights against the observations in the Amazon basin (a, ALF; b, RBA; c, SAN; d, TAB_TEF).

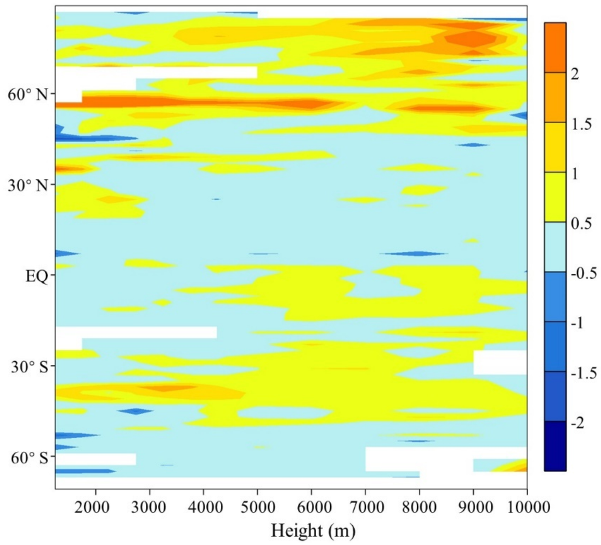

Figure 13: BIAS at different latitudes and heights against the HIPPO observations.

Table 1: Global carbon budget (PgC yr^{-1}).

Year	NEE	OCN flux	FFC emission	FIRE emission	Net Flux
2010	-3.28±0.49	-2.11±0.15	9.04	2.15	5.80±0.51
2011	-5.24±0.50	-2.21±0.15	9.40	1.87	3.81±0.52
2012	-3.77±0.50	-2.27±0.15	9.58	2.05	5.58±0.52
2013	-4.13±0.49	-2.40±0.15	9.63	1.77	4.86±0.51
2014	-4.50±0.51	-2.46±0.16	9.71	2.04	4.79±0.53
2015	-3.50±0.53	-2.52±0.16	9.68	2.29	5.95±0.56
2016	-2.51±0.53	-2.73±0.16	9.71	1.87	6.33±0.56
2017	-3.74±0.56	-3.06±0.17	9.87	1.92	4.99±0.58
2018	-3.54±0.56	-3.37±0.16	10.07	1.83	4.99±0.58
2019	-3.04±0.49	-3.23±0.16	10.03	2.32	6.08±0.52
Mean	-3.73±0.52	-2.64±0.16	9.67	2.01	5.32±0.54

https://doi.org/10.5194/essd-2022-15
Preprint. Discussion started: 4 February 2022

Table 2: Regional terrestrial ecosystem carbon flux (PgC yr^{-1}).

TRANSCOM region	NEE	FIRE	NBE	RECCAP2 region	NEE	FIRE	NBE
Boreal N. America	-0.32±0.12	0.08	-0.23±0.12	N. America	-0.78±0.23	0.14	-0.64±0.23
Temperate N. America	-0.43±0.19	0.04	-0.40±0.19	S. America	-0.53±0.21	0.29	-0.24±0.22
Tropical S. America	-0.50±0.16	0.20	-0.30±0.16	Russia	-1.02±0.20	0.15	-0.87±0.20
Temperate S. America	-0.06±0.14	0.10	0.04±0.14	Europe*	-0.36±0.13	0.01	-0.35±0.13
Northern Africa	-0.03±0.21	0.37	0.34±0.21	West Asia	-0.05±0.03	0.01	-0.04±0.03
Southern Africa	-0.13±0.17	0.66	0.53±0.17	Africa	-0.17±0.27	1.03	0.87±0.27
Boreal Asia	-0.68±0.18	0.14	-0.54±0.18	East Asia	-0.30±0.15	0.03	-0.27±0.15
Temperate Asia	-0.32±0.17	0.04	-0.29±0.17	South Asia	-0.07±0.10	0.02	-0.05±0.10
Tropical Asia	-0.32±0.09	0.20	-0.12±0.09	Southeast Asia	-0.25±0.08	0.19	-0.06±0.08
Australia	-0.12±0.06	0.12	0.00±0.06	Australasia	-0.12±0.06	0.12	0.00±0.06
Europe	-0.72±0.17	0.02	-0.70±0.17	-	-	-	-

*Excluding European Russia